A novel bond-based nonlocal diffusion model with matrix-valued coefficients in non-divergence form and its collocation discretization

Hao Tian[a], Junke Lu[a], Lili Ju[b,*]

[a] *School of Mathematical Sciences, Ocean University of China, Qingdao, Shandong 266100, China.*
[b] *Department of Mathematics, University of South Carolina, Columbia, SC 29208, USA.*

Abstract

Existing nonlocal diffusion models are mainly classified into two categories: bond-based models, which involve a single-fold integral and usually simulate isotropic diffusion, and state-based models, which contain a double-fold integral and can additionally prototype anisotropic diffusion. While bond-based models exhibit more computational efficiency, they sometimes could be limited in modeling capabilities. In this paper, we successfully develop a novel bond-based nonlocal model for the diffusion process with matrix-valued coefficients in non-divergence form. Our approach incorporates the coefficients into a covariance matrix and employs the multivariate Gaussian function with truncation to define the kernel function, and subsequently model the nonlocal diffusion through the bond-based formulation. We establish the well-posedness of the proposed model along with deriving some of its properties on maximum principle and mass conservation. Furthermore, an efficient linear collocation scheme is designed for numerical solution of our model. Comprehensive experiments in two and three dimensions are conducted to showcase application of the proposed nonlocal model to both isotropic and anisotropic diffusion problems, and to demonstrate high-order accuracy and conditional δ-convergence of the proposed collocation scheme.

Keywords: Nonlocal model, anisotropic diffusion, bond-based model, Gaussian function, collocation scheme, asymptotic compatibility

1. Introduction

Isotropic and anisotropic diffusion phenomena have received much attention due to their broad applications, such as inertial confinement fusion (ICF) [30, 36], magnetic confinement fusion (MCF) [45], skyrmion diffusion in magnetism [28], image processing [35, 48], gas diffusion in fractal porous media [33], and fluid distribution in fiber-reinforced composites [21]. These diffusion processes are usually described by partial differential equations (PDEs), for examples, Fick's law [44], Darcy's law [46] and Fourier's law [20]. The study of these equations is of great interest in numerous scientific fields due to the importance of diffusion processes in physical systems. The linear diffusion equation

*H. Tian's work is partially supported by Chinese Fundamental Research Funds for the Central Universities 202264006 and National Natural Science Foundation of China grants 11801533 and 11971482. L. Ju's work is partially supported by U.S. National Science Foundation grant DMS-2109633.

*Corresponding author.

Email addresses: haot@ouc.edu.cn (Hao Tian), lujunke@stu.ouc.edu.cn (Junke Lu), ju@math.sc.edu (Lili Ju)

with matrix-valued coefficients in non-divergence form is given by

$$-\mathcal{L}u(\boldsymbol{x}) := -\sum_{i,j=1}^{d} a^{i,j}(\boldsymbol{x})\frac{\partial^2 u}{\partial x_i \partial x_j}(\boldsymbol{x}) = f(\boldsymbol{x}), \quad \boldsymbol{x} \in \Omega, \tag{1.1}$$

where $\Omega \in \mathbb{R}^d$ is a bounded Lipschitz domain, $u(\boldsymbol{x}) : \Omega \to \mathbb{R}$ is the unknown function, and the coefficient matrix $\mathbf{A}(\boldsymbol{x}) = \left(a^{i,j}(\boldsymbol{x})\right)_{i,j=1}^{d}$ is assumed to be elliptic, i.e., symmetric and positive definite and

$$\lambda|\boldsymbol{\xi}|^2 \leq \boldsymbol{\xi}^T \mathbf{A}(\boldsymbol{x})\boldsymbol{\xi} \leq \Lambda|\boldsymbol{\xi}|^2, \quad \forall\, \boldsymbol{\xi} \in \mathbb{R}^d, \boldsymbol{x} \in \Omega, \tag{1.2}$$

where λ and Λ are some positive constants. The diffusion process is said to be *isotropic* if $\mathbf{A}(\boldsymbol{x}) = a(\boldsymbol{x})\mathbf{I}$ where $a(\boldsymbol{x})$ is a scalar-valued coefficient function and $\mathbf{I}$ denotes the identity matrix, and otherwise it is said to be *anisotropic*. For the well-posedness of the problem (1.1), we refer to the comprehensive analysis and results presented in [23]. For simplicity, we assume $a^{i,j}(\boldsymbol{x}) \in C^{0,1}(\Omega)$ and $f \in L^2(\Omega)$ in this paper, which guarantees the existence and uniqueness of a solution for (1.1) under the Dirichlet boundary condition. This type of equations have been used in many applications, such as stochastic optimal control and finance [19], the optimal transportation problem and geometry [5, 31, 42], the linearized fully nonlinear problems [3, 34]. Since analytic solutions are usually unavailable in practice, many numerical methods have been developed to solve the equation (1.1), including the finite volume (FV) schemes [38, 47, 49], the finite volume element (FVE) method [22, 29, 39] and so on.

It is known that classical diffusion models described by PDEs often cannot provide a proper description of diffusion through heterogeneous materials, and they are limited in describing anomalous diffusion that does not obey Fick's law. Nonlocal diffusion model is an alternative to the PDE-based diffusion equation, which is based on Silling's reformulation of the theory of elasticity for solid mechanic [37, 40]. Bond-based models (i.e., unweighted nonlocal models) and state-based models (i.e., weighted nonlocal models) are the two major types of nonlocal diffusion models [11, 13, 17, 24]. the former ones are independent on the influence of other points in their domain of interaction and the latter ones are opposite.

In the past two decades nonlocal diffusion models based on integral equations have gained extensive attention [12, 15, 32]. The literature contains advanced engineering applications of nonlocal diffusion equations. For instance, some studies have explored the peridynamic formulation for heat transfer, including one-dimensional problems with different boundary conditions [1]. Other studies have introduced multidimensional peridynamic formulations for transient heat transfer [2], and refined bond-based peridynamic approaches for thermo-mechanical coupling problems [6]. State-based peridynamic heat conduction equations and their applications were also investigated, with examples including the use of peridynamic differential operators for steady-state heat conduction analysis in plates with insulated cracks [10] and the nonlocal discrete model based on the lattice particle method for modeling anisotropic heat conduction [7]. Nonlocal diffusion models also have been applied in fluid transport in porous media and corrosion. For example, state-based peridynamic formulations were developed to simulate convective transport of single-phase flow and transient moisture flow through heterogeneous and anisotropic porous media, as in [27] and [26], respectively. Nonlocal fluid transport models were proposed to capture the non-local transport effects and non-linear mechanical behaviors of fluids in heterogeneous saturated porous media [41]. In the area of corrosion, a variety of coupled mechano-chemical peridynamic models were developed

to describe stress-assisted corrosion and stress corrosion cracking; specific examples include models introduced in [12, 25, 50], which presents a coupled peridynamic corrosion-fracture model.

A stated-based nonlocal model was successfully proposed and analyzed to simulate the anisotropic diffusion in [9], but it is theoretically not necessary to use the state-based formulation for modeling anisotropic diffusion. In [13], a connection between the bond-based nonlocal model and the general diffusion process was established: the bond-based nonlocal diffusion operator based on the radial-type kernel function $\gamma(|\mathbf{z}|)$ with a compact support $B_\delta(\mathbf{0})$ converges to $-\nabla\cdot(\mathbf{A}\,\nabla)$ as the horizon parameter $\delta\to 0$ under suitable conditions on $\gamma(|\mathbf{z}|)$. However, to the best of our knowledge, such kernel function $\gamma(|\mathbf{z}|)$ has not been found in the literature when $\mathbf{A}$ is anisotropic.

In this paper, we successfully develop a novel bond-based nonlocal model which can simulate both isotropic and anisotropic diffusion processes. Our approach incorporates the coefficient matrix into a covariance matrix and then forms the kernel function based on the multivariate Gaussian function. To ensure computational efficiency in practice, we further appropriately truncate the influence region of the kernel function by considering its rapid decaying nature. We establish the well-posedness of the proposed model under certain assumption on the coefficient matrix, and derive its maximum principle, and when $\mathbf{A}$ is a constant matrix, the mass conservation. An efficient linear collocation discretization scheme is also proposed for numerical solution of our model, which is shown to converge exponentially on uniform rectangular grids and quadratically non-uniform grids. In terms of asymptotic compatibility, we observe through extensive numerical experiments that the proposed collocation scheme is δ-convergent under a reasonable condition on the ratio of the horizon parameter over the grid size, while the popular quadrature-based finite difference scheme [16, 14] fails in the case of anisotropic coefficients.

The rest of the paper is organized as follows. Section 2 briefly reviews some existing nonlocal models for isotropic and anisotropic diffusion. Section 3 introduces the new bond-based nonlocal diffusion model with matrix-valued coefficients and discusses the truncation of the influence region of the kernel function for its efficient implementation in practice. Section 4 establishes the well-posedness of the proposed model and derive some of its properties. Section 5 presents the linear collocation discretization scheme for numerical solution of our model. Section 6 provides extensive numerical experiments in two and three dimensions to illustrate application of our model to various isotropic and anisotropic diffusion problems and to demonstrate numerical accuracy and conditional δ-convergence of the proposed collocation scheme. Some conclusions are finally given in Section 7.

2. Review of existing nonlocal diffusion models

2.1. Nonlocal modeling for isotropic diffusion

Within the framework of nonlocal vector calculus [13], given $\boldsymbol{\nu}(\boldsymbol{x},\boldsymbol{y}):\mathbb{R}^d\times\mathbb{R}^d\to\mathbb{R}^d$, the *unweighted nonlocal divergence operator* $\mathcal{D}$ acting on $\boldsymbol{\nu}$ is defined as

$$\mathcal{D}\boldsymbol{\nu}(\boldsymbol{x}) := \int_{\mathbb{R}^d} (\boldsymbol{\nu}(\boldsymbol{x},\boldsymbol{y}) + \boldsymbol{\nu}(\boldsymbol{y},\boldsymbol{x}))\cdot\boldsymbol{\alpha}(\boldsymbol{x},\boldsymbol{y})\,d\boldsymbol{y}, \tag{2.1}$$

where $\boldsymbol{\alpha}(\boldsymbol{x},\boldsymbol{y}):\mathbb{R}^d\times\mathbb{R}^d\to\mathbb{R}^d$ is a pre-determined antisymmetric vector, i.e. $\boldsymbol{\alpha}(\boldsymbol{x},\boldsymbol{y}) = -\boldsymbol{\alpha}(\boldsymbol{y},\boldsymbol{x})$. For any $u(\boldsymbol{x}):\mathbb{R}^d\to\mathbb{R}$, the unweighted adjoint (i.e., nonlocal gradient) operator $\mathcal{D}^*$ corresponding to $\mathcal{D}$ is then defined as

$$\mathcal{D}^* u(\boldsymbol{x},\boldsymbol{y}) := (u(\boldsymbol{y}) - u(\boldsymbol{x}))\boldsymbol{\alpha}(\boldsymbol{x},\boldsymbol{y}). \tag{2.2}$$

Let $\Theta(\boldsymbol{x},\boldsymbol{y}):\mathbb{R}^d\times\mathbb{R}^d\to\mathbb{R}^{d\times d}$ be a symmetric positive definite matrix-valued function. Under the above definitions of $\mathcal{D}$ and $\mathcal{D}^*$, we have

$$\mathcal{D}(\Theta\cdot\mathcal{D}^*u)(\boldsymbol{x})=2\int_{\mathbb{R}^d}(u(\boldsymbol{y})-u(\boldsymbol{x}))\alpha(\boldsymbol{x},\boldsymbol{y})\cdot(\Theta(\boldsymbol{x},\boldsymbol{y})\cdot\boldsymbol{\alpha}(\boldsymbol{x},\boldsymbol{y}))\,d\boldsymbol{y}. \tag{2.3}$$

If we define the kernel function $\gamma(\boldsymbol{x},\boldsymbol{y})=2\alpha\cdot(\Theta\cdot\alpha)$, which is clearly nonnegative and symmetric, then (2.3) also can be written as

$$\mathcal{D}(\Theta\cdot\mathcal{D}^*u)(\boldsymbol{x})=\int_{\mathbb{R}^d}(u(\boldsymbol{y})-u(\boldsymbol{x}))\gamma(\boldsymbol{x},\boldsymbol{y})\,d\boldsymbol{y}. \tag{2.4}$$

Let us take

$$\boldsymbol{\alpha}(\boldsymbol{x},\boldsymbol{y})=\frac{\boldsymbol{y}-\boldsymbol{x}}{\|\boldsymbol{y}-\boldsymbol{x}\|},\quad \Theta(\boldsymbol{x},\boldsymbol{y})=a(\boldsymbol{x})\omega(\boldsymbol{x},\boldsymbol{y})\mathbf{I},$$

where $a(\boldsymbol{x}):\mathbb{R}^d\to\mathbb{R}$ is the scalar-valued diffusion coefficient and $\omega(\boldsymbol{x},\boldsymbol{y})=\omega(\|\boldsymbol{y}-\boldsymbol{x}\|):\mathbb{R}^d\times\mathbb{R}^d\to\mathbb{R}$ is the influence function with a compact support $B_\delta(\boldsymbol{x})=\{\boldsymbol{y}:\|\boldsymbol{y}-\boldsymbol{x}\|\le\delta\}$ (the horizon parameter $\delta>0$). Then we have a bond-based nonlocal isotropic diffusion model as follows:

$$\begin{aligned}\mathcal{D}(\Theta\cdot\mathcal{D}^*u)(\boldsymbol{x}) &= \int_{\mathbb{R}^d}(u(\boldsymbol{y})-u(\boldsymbol{x}))\frac{(\boldsymbol{y}-\boldsymbol{x})^T}{\|\boldsymbol{y}-\boldsymbol{x}\|}\cdot(a(\boldsymbol{x})\mathbf{I}+a(\boldsymbol{y})\mathbf{I})\cdot\frac{\boldsymbol{y}-\boldsymbol{x}}{\|\boldsymbol{y}-\boldsymbol{x}\|}\omega(\boldsymbol{x},\boldsymbol{y})\,d\boldsymbol{y}\\ &= \int_{B_\delta(\boldsymbol{x})}(u(\boldsymbol{y})-u(\boldsymbol{x}))\gamma(\boldsymbol{x},\boldsymbol{y})\,d\boldsymbol{y},\end{aligned} \tag{2.5}$$

where $\gamma(\boldsymbol{x},\boldsymbol{y})=(a(\boldsymbol{x})+a(\boldsymbol{y}))\omega(\boldsymbol{x},\boldsymbol{y})$. It is shown [17] that as δ goes to 0, the nonlocal diffusion operator, $\mathcal{D}(\Theta\cdot\mathcal{D}^*u)$, converge to the classic isotropic diffusion operator in divergence form, $\nabla\cdot(a(\boldsymbol{x})\nabla u)$.

2.2. Nonlocal modeling for anisotropic diffusion

A ω-weighted nonlocal divergence operator [13] acting on $\boldsymbol{\mu}(\boldsymbol{x}):\mathbb{R}^d\to\mathbb{R}^d$ is defined as

$$\mathcal{D}_\omega\boldsymbol{\mu}(\boldsymbol{x}):=\mathcal{D}(\omega\boldsymbol{\mu})(\boldsymbol{x}). \tag{2.6}$$

The ω-weighted nonlocal gradient operator $\mathcal{D}_\omega^*$ corresponding to $\mathcal{D}_\omega$ is correspondingly defined as

$$\mathcal{D}_\omega^*u(\boldsymbol{x}):=\int_{\mathbb{R}^d}\omega(\boldsymbol{x},\boldsymbol{y})\mathcal{D}^*u(\boldsymbol{x},\boldsymbol{y})\,d\boldsymbol{y}. \tag{2.7}$$

Then a state-based nonlocal anisotropic diffusion model can be defined as follows:

$$\begin{aligned}\mathcal{D}_\omega(\mathbf{A}\cdot\mathcal{D}_\omega^*u)(\boldsymbol{x}) &= \int_{\mathbb{R}^d}\big[\mathbf{A}(\boldsymbol{x})\int_{\mathbb{R}^d}\omega(\boldsymbol{x},\boldsymbol{z})\mathcal{D}^*u(\boldsymbol{x},\boldsymbol{z})d\boldsymbol{z}\\ &\quad+\mathbf{A}(\boldsymbol{y})\int_{\mathbb{R}^d}\omega(\boldsymbol{y},\boldsymbol{z})\mathcal{D}^*u(\boldsymbol{y},\boldsymbol{z})d\boldsymbol{z})\big]\cdot\alpha(\boldsymbol{x},\boldsymbol{y})\omega(\boldsymbol{x},\boldsymbol{y})d\boldsymbol{y}.\end{aligned} \tag{2.8}$$

Note that the state-based model includes a two-fold integral while the bond-based one doesn't. Thus the bond-based one is usually more efficient in terms of computational cost. With Taylor expansion, one can show that as δ goes to 0, the nonlocal diffusion operator, $\mathcal{D}_\omega(\mathbf{A}(\boldsymbol{x})\cdot\mathcal{D}_\omega^*u)$, converges to the classic anisotropic diffusion operator in divergence form, $\nabla\cdot(\mathbf{A}(\boldsymbol{x})\nabla u)$. It has

been pointed out that under the suitable conditions on the kernel function $\gamma(\boldsymbol{x},\boldsymbol{y})$, the bond-based nonlocal model (2.4) also can be employed to simulate anisotropic diffusion. Assume that the kernel function is radially symmetric (i.e., $\gamma(\boldsymbol{x},\boldsymbol{y})=\gamma(|\boldsymbol{y}-\boldsymbol{x}|)$) and satisfies

$$a^{i,j}=\lim_{\delta\to 0}\int_{B_\delta(0)}\gamma(|\mathbf{z}|)z_iz_jd\mathbf{z},\quad \text{for}\quad i,j=1,2,\ldots,d, \tag{2.9}$$

then the nonlocal operator (2.4) converges to the classic diffusion operator $\nabla\cdot(\mathbf{A}\nabla u)$ as δ goes to 0 [13]. Unfortunately, such a suitable kernel function has not yet been successfully constructed (i.e., appropriate choice of $\boldsymbol{\alpha}$ and Θ) in the literature.

3. A novel bond-based nonlocal diffusion model with matrix-valued coefficients

In this section, we will first present the bond-based nonlocal diffusion model and then establish its well-posedness and some of its properties.

3.1. A nonlocal operator based on the Gaussian-type kernel function

Let $p(\boldsymbol{z},\boldsymbol{\mu},\boldsymbol{\Sigma})$ be the probability density function of the d-dimensional multivariate Gaussian (or normal) distribution with expectation vector $\boldsymbol{\mu}$ and covariance matrix $\boldsymbol{\Sigma}$, which is defined by

$$p(\boldsymbol{z},\boldsymbol{\mu},\Sigma)=\frac{1}{\sqrt{(2\pi)^d\,|\boldsymbol{\Sigma}|}}\exp\left(-\frac{1}{2}(\boldsymbol{z}-\boldsymbol{\mu})^T\boldsymbol{\Sigma}^{-1}(\boldsymbol{z}-\boldsymbol{\mu})\right). \tag{3.1}$$

We first propose and study a nonlocal diffusion operator with the coefficient matrix $\mathbf{A}$ defined as follows:

$$\mathcal{L}_\delta u(\boldsymbol{x}):=\int_{\mathbb{R}^d}(u(\boldsymbol{y})-u(\boldsymbol{x}))\gamma(\boldsymbol{x},\boldsymbol{y})\,d\boldsymbol{y},\quad \boldsymbol{x}\in\mathbb{R}^d, \tag{3.2}$$

where the kernel function $\gamma(\boldsymbol{x},\boldsymbol{y})$ is defined as

$$\gamma(\boldsymbol{x},\boldsymbol{y})=\frac{2}{\delta^2}p(\boldsymbol{y}-\boldsymbol{x},\mathbf{0},\delta^2\mathbf{A}(\boldsymbol{x})). \tag{3.3}$$

It is clear that $\gamma(\boldsymbol{x},\boldsymbol{y})>0$ and has an unbounded support region for any $\boldsymbol{x}\in\mathbb{R}^d$. Instead of acting directly as the horizon's radius in the traditional bond-based nonlocal models, here the parameter δ is used in constructing the covariance matrix. Note that as δ gets smaller, the kernel function $\gamma(\boldsymbol{x},\boldsymbol{y})$ would get more singular, as illustrated in Figure 1 for some two dimensional cases. Another important difference with traditional nonlocal models is that the coefficient matrix $\mathbf{A}(\boldsymbol{x})$ is directly incorporated into and impact the kernel function, as illustrated in Figure 2. Although the influence region of $\gamma(\boldsymbol{x},\boldsymbol{y})$ for a point $\boldsymbol{x}$ is the whole space $\boldsymbol{x}\in\mathbb{R}^d$ theoretically, but the magnitude of the interaction between $\boldsymbol{x}$ and other point $\boldsymbol{y}$ quickly shrinks to 0 when $\boldsymbol{x}$ and $\boldsymbol{y}$ get aways with each other.

Let us denote the domain in which the nonlocal operator is applied by Ω_s, and then the nonlocal diffusion problem associated with the operator $\mathcal{L}_\delta$ under the Dirichlet-type boundary condition is given by:

$$\begin{cases}-\mathcal{L}_\delta u(\boldsymbol{x})=f(\boldsymbol{x}), & \boldsymbol{x}\in\Omega_s,\\ \quad u(\boldsymbol{x})=g(\boldsymbol{x}), & \boldsymbol{x}\in\mathbb{R}^d\setminus\Omega_s.\end{cases} \tag{3.4}$$

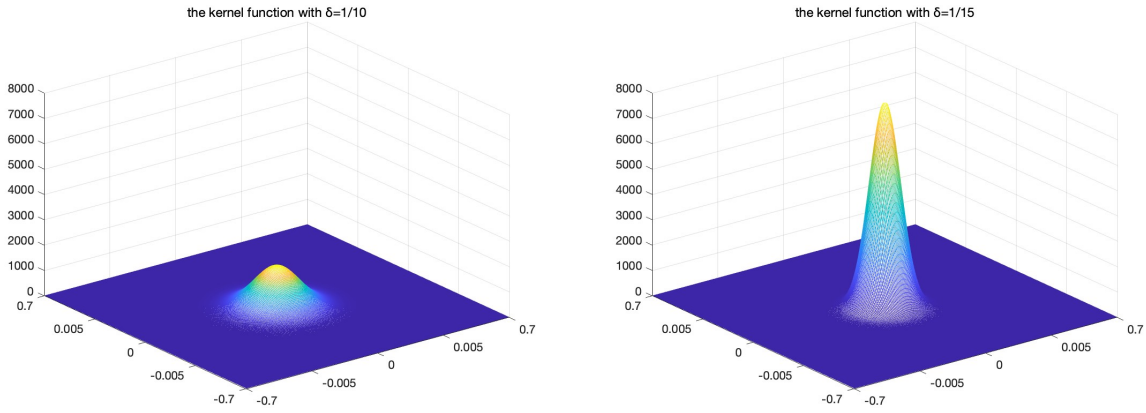

Figure 1: *Plots of the kernel function* $\gamma(\boldsymbol{x}, \boldsymbol{y})$ *in two dimensions with the isotropic constant coefficient matrix* $\mathbf{A} = [1, 0; 0, 1]$ *and* $\delta = 1/10$ *(left) and* $\delta = 1/15$ *(right), respectively. A smaller* δ *results in contours that are more elongated and concentrated around the center, while a larger* δ *leads to contours that are more spread out and diffuse.*

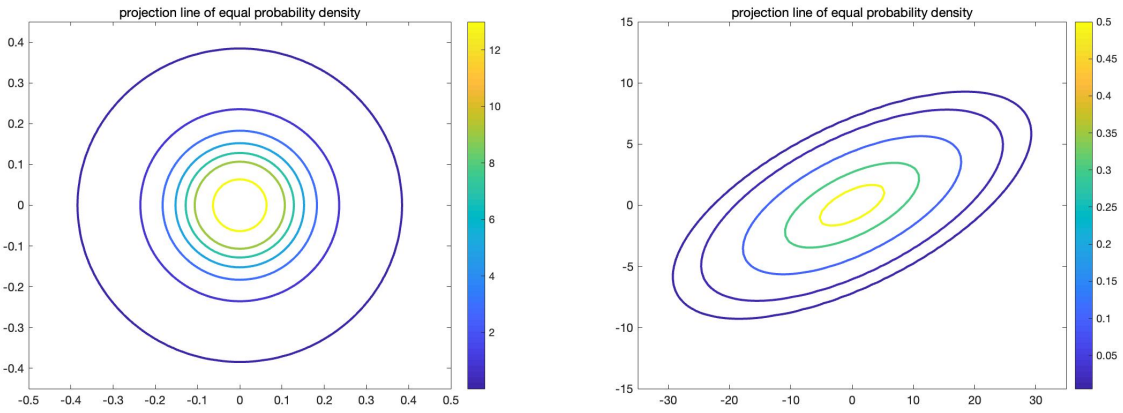

Figure 2: *When the diffusion coefficient matrix* $\mathbf{A} = [1, 0; 0, 1]$*, the probability density function is isotropic and thus the projection of its iso-density contours onto the coordinate plane takes the form of a circle (left). When the diffusion coefficient matrix* $\mathbf{A} = [10, 2; 2, 1]$*, the probability density function is anisotropic and subjected to a combined stretching and rotation, resulting in the rotated image of an elliptical shape upon projection onto the coordinate plane (right).*

3.2. Convergence to the local diffusion operator in non-divergence form

Suppose the solution u is sufficiently smooth. By applying Taylor expansion at $\boldsymbol{x} \in \Omega_s$, we obtain that for any $\boldsymbol{y} \in \mathbb{R}^d$,

$$\begin{aligned} u(\boldsymbol{y}) - u(\boldsymbol{x}) = \nabla u(\boldsymbol{x})^T(\boldsymbol{y} - \boldsymbol{x}) + \frac{1}{2!}(\boldsymbol{y} - \boldsymbol{x})^T \mathbf{H}_u(\boldsymbol{x})(\boldsymbol{y} - \boldsymbol{x}) \\ + \sum_{p,q,r=1}^{d} \frac{1}{3!} \frac{\partial^3 u(\boldsymbol{x})}{\partial x_p \partial x_q \partial x_r} (\boldsymbol{y} - \boldsymbol{x})_p (\boldsymbol{y} - \boldsymbol{x})_q (\boldsymbol{y} - \boldsymbol{x})_r + \cdots, \end{aligned} \tag{3.5}$$

where the matrix $\mathbf{H}_u$ is the Hessians of u. Then by putting (3.5) into (3.2), we have:

$$\begin{aligned}\int_{\mathbb{R}^d}(u(\boldsymbol{y})-u(\boldsymbol{x}))\gamma(\boldsymbol{x},\boldsymbol{y})d\boldsymbol{y} &= \int_{\mathbb{R}^d}\nabla u(\boldsymbol{x})^T(\boldsymbol{y}-\boldsymbol{x})\gamma(\boldsymbol{x},\boldsymbol{y})d\boldsymbol{y}\\ &+\int_{\mathbb{R}^d}\frac{1}{2!}(\boldsymbol{y}-\boldsymbol{x})^T\mathbf{H}_u(\boldsymbol{x})(\boldsymbol{y}-\boldsymbol{x})\gamma(\boldsymbol{x},\boldsymbol{y})d\boldsymbol{y}\\ &+\int_{\mathbb{R}^d}\sum_{p,q,r=1}^{d}\frac{1}{3!}\frac{\partial^3 u(\boldsymbol{x})}{\partial x_p\partial x_q\partial x_r}(\boldsymbol{y}-\boldsymbol{x})_p(\boldsymbol{y}-\boldsymbol{x})_q(\boldsymbol{y}-\boldsymbol{x})_r\gamma(\boldsymbol{x},\boldsymbol{y})d\boldsymbol{y}+\cdots.\end{aligned} \tag{3.6}$$

According to the definition of moments for the multivariate Gaussian distribution [4], it is easy to see that the integrals of the first and third terms of the right-hand side of (3.6) are 0, i.e.,

$$\int_{\mathbb{R}^d}\nabla u(\boldsymbol{x})^T(\boldsymbol{y}-\boldsymbol{x})\gamma(\boldsymbol{x},\boldsymbol{y})\,d\boldsymbol{y}=0, \tag{3.7}$$

and

$$\int_{\mathbb{R}^d}\sum_{p,q,r=1}^{d}\frac{1}{3!}\frac{\partial^3 u(\boldsymbol{x})}{\partial x_p\partial x_q\partial x_r}(\boldsymbol{y}-\boldsymbol{x})_p(\boldsymbol{y}-\boldsymbol{x})_q(\boldsymbol{y}-\boldsymbol{x})_r\gamma(\boldsymbol{x},\boldsymbol{y})d\boldsymbol{y}=0. \tag{3.8}$$

For the integral of the second term of the right-hand side of (3.5), we have the following equality:

$$\frac{1}{2}\int_{\mathbb{R}^d}(\boldsymbol{y}-\boldsymbol{x})_i(\boldsymbol{y}-\boldsymbol{x})_j\gamma(\boldsymbol{x},\boldsymbol{y})d\boldsymbol{y}=a^{i,j}(\boldsymbol{x}),\quad 1\le i,j\le d. \tag{3.9}$$

Finally, the nonlocal operator defined in (3.2) can be written as:

$$\mathcal{L}_\delta u(\boldsymbol{x})=\sum_{i,j=1}^{d}a^{i,j}(\boldsymbol{x})\frac{\partial^2 u}{\partial x_i\partial x_j}(\boldsymbol{x})+O(\delta^2), \tag{3.10}$$

where $O(\delta^2)$ is obtained by integrating the fourth-order remainder in Taylor expansion. Hence, as the horizon parameter $\delta\to 0$, the nonlocal operator $\mathcal{L}_\delta$ converges to the local diffusion operator in non-divergence form defined in (1.1), i.e.,

$$\mathcal{L}_\delta u(\boldsymbol{x})\to\mathcal{L}u(\boldsymbol{x}):=\sum_{i,j=1}^{d}a^{i,j}(\boldsymbol{x})\frac{\partial^2 u}{\partial x_i\partial x_j}(\boldsymbol{x}).$$

Furthermore, the convergence is expected to be quadratically with respect to δ. Thus the partial differential equation problem, as the local counterpart of the nonlocal diffusion problem (3.4), is given by

$$\begin{cases}-\mathcal{L}u(\boldsymbol{x})=f(\boldsymbol{x}), & \boldsymbol{x}\in\Omega_s,\\ \quad u(\boldsymbol{x})=g(\boldsymbol{x}), & \boldsymbol{x}\in\partial\Omega_s.\end{cases} \tag{3.11}$$

In the case of constant coefficient matrix $\mathbf{A}$, we further have $\mathcal{L}_\delta u\to\nabla\cdot(\mathbf{A}\nabla)u$ since $\frac{\partial\mathbf{A}}{\partial x_i}\equiv\mathbf{0}$.

3.3. Truncation of the influence region for the kernel function

The nonlocal model (3.2) utilizes a kernel function $\gamma(\boldsymbol{x}, \boldsymbol{y})$ for $\mathcal{L}_\delta$ defined over an unbounded area, which presents computational challenges for practical implementation. However, due to the rapid (exponentially) decay of the kernel function γ when $\boldsymbol{y}$ gets away from the given point $\boldsymbol{x} \in \Omega_s$, it is feasible to truncate the influence region of $\gamma(\boldsymbol{x}, \boldsymbol{y})$ to ensure computational efficiency in practice. By choosing a suitable cut-off distance, one can effectively limit the computational domain to a finite region with just negligible loss of the model accuracy. This way allows for the application of the proposed nonlocal model in a more practical manner, while still capturing the essential physics of the system under consideration.

As is known that with any fixed $\boldsymbol{x}$, if $\boldsymbol{y} - \boldsymbol{x}$ follows the d-dimensional mean-zero Gaussian distribution with covariance matrix $\delta^2 \mathbf{A}(\boldsymbol{x})$, it holds that $(\boldsymbol{y} - \boldsymbol{x})^T \mathbf{A}(\boldsymbol{x})^{-1} (\boldsymbol{y} - \boldsymbol{x})/\delta^2$ obey the chi-square distribution $\chi^2(d)$ [4]. If we take the influence region of the kernel function at $\boldsymbol{x}$ to just include all $\boldsymbol{y}$ such that $(\boldsymbol{y} - \boldsymbol{x})^T \mathbf{A}(\boldsymbol{x})^{-1} (\boldsymbol{y} - \boldsymbol{x}) \leq \delta^2 \chi^2_\alpha(d)$, where $0 < \alpha \ll 1$ is a predetermined constant parameter and $\chi^2_\alpha(d)$ denotes the $(1-\alpha)$ quantile of the chi-square distribution, then we have

$$\int \cdots \int_{(\boldsymbol{y}-\boldsymbol{x})^T \mathbf{A}(\boldsymbol{x})^{-1} (\boldsymbol{y}-\boldsymbol{x}) \leq \delta^2 \chi^2_\alpha(d)} p(\boldsymbol{y} - \boldsymbol{x}, \mathbf{0}, \delta^2 \mathbf{A}(\boldsymbol{x}))\, d\boldsymbol{y} = 1 - \alpha. \tag{3.12}$$

We will take

$$B_{\delta, \mathbf{A}, \alpha}(\boldsymbol{x}) = \{\boldsymbol{y} \mid (\boldsymbol{y} - \boldsymbol{x})^T \mathbf{A}(\boldsymbol{x})^{-1} (\boldsymbol{y} - \boldsymbol{x}) \leq \delta^2 \chi^2_\alpha(d)\} \tag{3.13}$$

as the truncated influence region for $\boldsymbol{x}$ with α selected very close to 0. Figure 3 illustrates the projection of iso-density contour of the truncated influence region onto the coordinate plane for different coefficient matrices in two dimensions, where $\chi^2_\alpha(2) = 36$, that is $\alpha \approx 1.52 \times 10^{-8}$. For the identity matrix, the contour takes on a circular shape, as shown on the left-hand side of the figure. For other matrices, such as those involving stretching and rotation, the contours may appear as rotated ellipses. Overall, the shape of the iso-density contours provides insight into the nature of the underlying probability density function for the kernel function and the effect of the transformation matrix on its properties. Thus, we correspondingly define the truncated kernel function γ_α as: for any $\boldsymbol{x}, \boldsymbol{y} \in \mathbb{R}^d$,

$$\gamma_\alpha(\boldsymbol{x}, \boldsymbol{y}) = \begin{cases} \gamma(\boldsymbol{x}, \boldsymbol{y}), & \boldsymbol{y} \in B_{\delta, \mathbf{A}, \alpha}(\boldsymbol{x}), \\ 0, & \text{otherwise.} \end{cases} \tag{3.14}$$

Note that the identities (3.7) and (3.8) still hold exactly for the above truncated kernel function $\gamma_\alpha(\boldsymbol{x}, \boldsymbol{y})$, but the equality (3.9) doesn't and its error depends on the choice of α and converges to 0 as δ goes to 0.

In the context of nonlocal operators, it is common to impose constraints on certain interaction domain Ω_c, which has a positive volume. These volume constraints are the natural extensions of boundary conditions commonly used in differential equation problems. By specifying appropriate volume constraints, one can effectively control the behavior of the nonlocal operator in Ω_s, thereby ensuring the desired properties of the solution. For example, such constraints may include restrictions on the overall quality or energy of the system, or restrictions on the nonlocal kernel function support. In this way, volume constraints offer a powerful tool for designing and optimizing nonlocal operator models, and have wide-ranging applications in the study of physical systems and processes. Given the domain $\Omega_s \in \mathbb{R}^d$, we define the corresponding interaction domain associated

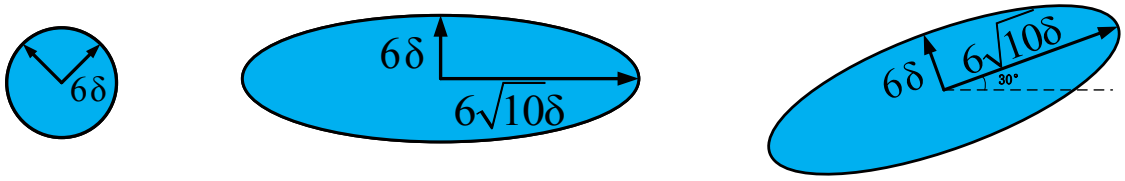

(a) (b) (c)

Figure 3: *Illustration of the truncated influence region* $B_{\delta,\mathbf{A},\alpha}(\mathbf{0})$ *with* $\chi^2_\alpha(2) = 36$ *(i.e.,* $\alpha \approx 1.52 \times 10^{-8}$*) in two dimensions. Left: the identity coefficient matrix* $\mathbf{A} = [1, 0; 0, 1]$*, the truncated influence region is a disk with radius* 6δ*; middle: an anisotropic coefficient matrix* $\mathbf{A} = [10, 0; 0, 1]$*, the truncated influence region is an elliptic region whose semi-major axis is* $6\sqrt{10}\delta$ *and semi-minor axis is* 6δ*; right:* $\mathbf{A} = [31/4, -9\sqrt{3}/4; -9\sqrt{3}/4, 13/4]$*, the truncated influence region of is a rotated (counterclockwisely* $30°$*) elliptic region whose semi-major axis is* $6\sqrt{10}\delta$ *and semi-minor axis is* 6δ*.*

with the kernel function γ_α as

$$\Omega_c := \left\{ \boldsymbol{y} \in \mathbb{R}^d \setminus \Omega_s \mid \exists\, \boldsymbol{x} \in \Omega_s,\ \boldsymbol{y} \in B_{\delta,\mathbf{A},\alpha}(\boldsymbol{x}) \right\},$$

and the corresponding truncated nonlocal diffusion operator as

$$\mathcal{L}_{\delta,\alpha} u(\boldsymbol{x}) := \int_{\mathbb{R}^d} (u(\boldsymbol{y}) - u(\boldsymbol{x}))\gamma_\alpha(\boldsymbol{x}, \boldsymbol{y})\, d\boldsymbol{y}, \quad \boldsymbol{x} \in \Omega_s. \tag{3.15}$$

We remark that the nonlocal diffusion operator $\mathcal{L}_{\delta,\alpha} u(\boldsymbol{x})$ is an approximation of the original nonlocal diffusion operator $\mathcal{L}_\delta u(\boldsymbol{x})$, and $\mathcal{L}_{\delta,\alpha} u(\boldsymbol{x})$ converges to $\mathcal{L}_\delta u(\boldsymbol{x})$ quickly as α goes to 0, as shown in [4]. Finally, we obtain the corresponding bond-based nonlocal diffusion problem under the volume constraint-based Dirichlet boundary condition as follow:

$$\begin{cases} -\mathcal{L}_{\delta,\alpha} u(\boldsymbol{x}) = f(\boldsymbol{x}), & \boldsymbol{x} \in \Omega_s, \\ u(\boldsymbol{x}) = g(\boldsymbol{x}), & \boldsymbol{x} \in \Omega_c, \end{cases} \tag{3.16}$$

where $\Omega = \Omega_c \cup \Omega_s$.

4. Wellposedness and properties

We now study the well-posedness of the bond-based nonlocal diffusion model (3.16). Let us define the constrained space $L^2_{n0}(\Omega) = \{u \in L^2(\Omega) \,|\, u = 0 \text{ on } \Omega_c\}$ and denote by $(\cdot, \cdot)$ the L^2 inner product. Assume $f \in L^2(\Omega_s)$. Then a weak formulation of the proposed nonlocal diffusion model (3.16) with the homogeneous boundary value $g|_{\Omega_c} = 0$ is given as follows: find $u \in L^2_{n0}(\Omega)$ such that

$$\mathbf{B}(u, v) = \mathbf{F}(v), \quad \forall\, v \in L^2_{n0}(\Omega)\,, \tag{4.1}$$

where

$$\mathbf{B}(u,v) = (-\mathcal{L}_{\delta,\alpha}u, v) = \int_\Omega \int_\Omega (u(\boldsymbol{x}) - u(\boldsymbol{y}))v(\boldsymbol{x})\gamma_\alpha(\boldsymbol{x},\boldsymbol{y})\, d\boldsymbol{y}d\boldsymbol{x},$$

and

$$\mathbf{F}(v) = \int_\Omega f(\boldsymbol{x})v(\boldsymbol{x})\, d\boldsymbol{x}.$$

Since $p(\boldsymbol{z}, \boldsymbol{\mu}, \boldsymbol{\Sigma})$ is a probability density function, it's easy to get

$$\int_\Omega \gamma(\boldsymbol{x},\boldsymbol{y})d\boldsymbol{y} = \frac{2}{\delta^2}. \tag{4.2}$$

Meanwhile, $\gamma_\alpha(\boldsymbol{x},\boldsymbol{y})$ is a truncated, scaled probability density function as defined in (3.14) with

$$\gamma_\alpha(\boldsymbol{x},\boldsymbol{y}) > 0, \quad \gamma_\alpha(\boldsymbol{y},\boldsymbol{x}) > 0, \tag{4.3}$$

and the coefficient matrix $\mathbf{A}$ is elliptic. It is not hard to see that the kernel γ_α satisfies: for any $\boldsymbol{x} \in \Omega$,

$$\begin{aligned} &\int_\Omega \gamma_\alpha(\boldsymbol{x},\boldsymbol{y})\, d\boldsymbol{y} \le \frac{2}{\delta^2}, \quad \int_\Omega \gamma_\alpha(\boldsymbol{y},\boldsymbol{x})\, d\boldsymbol{y} \le K_1(\delta), \\ &\int_{\Omega_c} \gamma_\alpha(\boldsymbol{x},\boldsymbol{y}) + \gamma_\alpha(\boldsymbol{y},\boldsymbol{x})\, d\boldsymbol{y} \ge K_2(\delta), \end{aligned} \tag{4.4}$$

where $K_1(\delta)$ and $K_2(\delta)$ are two positive constants depending on δ. Note that $\gamma_\alpha(\boldsymbol{x},\boldsymbol{y})$ isn't symmetric except when $\mathbf{A}(\boldsymbol{x})$ is a constant matrix, thus the bilinear operator $\mathbf{B}(u,v)$ is not symmetric in general. We then obtain the following result on the well-posedness of the nonlocal diffusion problem (3.16).

Theorem 1. (Well-posedness) *Let the parameter $\delta > 0$ be fixed. Assume that the kernel function $\gamma_\alpha(\boldsymbol{x},\boldsymbol{y})$ satisfies*

$$\int_\Omega \gamma_\alpha(\boldsymbol{x},\boldsymbol{y}) - \gamma_\alpha(\boldsymbol{y},\boldsymbol{x})\, d\boldsymbol{y} \ge 0, \quad \forall\, \boldsymbol{x} \in \Omega. \tag{4.5}$$

Then there exists a unique solution $u \in L^2_{n0}(\Omega)$ to the nonlocal diffusion problem (3.16)*. Furthermore, the solution satisfies the a priori estimate*

$$\|u\|_{L^2(\Omega)} \le \frac{4}{K_2(\delta)}\|f\|_{L^2(\Omega)}. \tag{4.6}$$

Proof. First, it is easy to see that $\mathbf{F}$ is a bounded linear functional:

$$|\mathbf{F}(v)| \le \|f\|_{L^2(\Omega)}\|v\|_{L^2(\Omega_s)}. \tag{4.7}$$

We now show that the bilinear operator $\mathbf{B}(\cdot,\cdot)$ is bounded on $L^2_{n0}(\Omega)\times L^2_{n0}(\Omega)$ by using a similar proof as that of Theorem 2 in [14]. For any $u, v \in L^2_{n0}(\Omega)$, it holds

$$\mathbf{B}(u,v) = \int_\Omega \int_\Omega u(\boldsymbol{x})v(\boldsymbol{x})\boldsymbol{\gamma}_\alpha(\boldsymbol{x},\boldsymbol{y})d\boldsymbol{y}d\boldsymbol{x} - \int_\Omega \int_\Omega u(\boldsymbol{y})v(\boldsymbol{x})\boldsymbol{\gamma}_\alpha(\boldsymbol{x},\boldsymbol{y})d\boldsymbol{y}d\boldsymbol{x} := I_1 - I_2. \tag{4.8}$$

Using the inequality in (4.4) and the Cauchy-Schwartz inequality, the first term of the right-hand side of (4.8) satisfies

$$|I_1| = \Big| \int_\Omega u(\boldsymbol{x})v(\boldsymbol{x}) \int_\Omega \boldsymbol{\gamma}_\alpha(\boldsymbol{x},\boldsymbol{y})\, d\boldsymbol{y}d\boldsymbol{x} \Big| \le \frac{2}{\delta^2}\|u\|_{L^2(\Omega)}\|v\|_{L^2(\Omega)},$$

and the second term of the right-hand side of (4.8) satisfies

$$\begin{aligned}|I_2| &\le \Big(\int_\Omega\int_\Omega u^2(\boldsymbol{y})\boldsymbol{\gamma}_\alpha(\boldsymbol{x},\boldsymbol{y})\,d\boldsymbol{y}d\boldsymbol{x}\Big)^{\frac{1}{2}}\Big(\int_\Omega\int_\Omega v^2(\boldsymbol{x})\boldsymbol{\gamma}_\alpha(\boldsymbol{x},\boldsymbol{y})\,d\boldsymbol{y}d\boldsymbol{x}\Big)^{\frac{1}{2}}\\ &\le \frac{\sqrt{2K_1(\delta)}}{\delta}\|u\|_{L^2(\Omega)}\|v\|_{L^2(\Omega)}.\end{aligned}$$

Thus we obtain

$$\mathbf{B}(u,v) \le |I_1| + |I_2| = \left(\frac{2}{\delta^2} + \frac{\sqrt{2K_1(\delta)}}{\delta}\right)\|u\|_{L^2(\Omega)}\|v\|_{L^2(\Omega)}. \tag{4.9}$$

Next we show that the bilinear operator $\mathbf{B}(\cdot,\cdot)$ is coercive on $L^2_{n0}(\Omega)$. Note that

$$\begin{aligned}\mathbf{B}(u,u) &= \int_\Omega\int_\Omega (u(\boldsymbol{x})-u(\boldsymbol{y}))\,u(\boldsymbol{x})\boldsymbol{\gamma}_\alpha(\boldsymbol{x},\boldsymbol{y})\,d\boldsymbol{y}d\boldsymbol{x}\\ &= \int_\Omega\int_\Omega (u(\boldsymbol{x})-u(\boldsymbol{y}))\,u(\boldsymbol{x})\frac{\boldsymbol{\gamma}_\alpha(\boldsymbol{x},\boldsymbol{y})+\boldsymbol{\gamma}_\alpha(\boldsymbol{y},\boldsymbol{x})}{2}\,d\boldsymbol{y}d\boldsymbol{x}\\ &\quad+\int_\Omega\int_\Omega (u(\boldsymbol{x})-u(\boldsymbol{y}))\,u(\boldsymbol{x})\frac{\boldsymbol{\gamma}_\alpha(\boldsymbol{x},\boldsymbol{y})-\boldsymbol{\gamma}_\alpha(\boldsymbol{y},\boldsymbol{x})}{2}\,d\boldsymbol{y}d\boldsymbol{x} := J_1+J_2.\end{aligned} \tag{4.10}$$

It is easy to see that $(\boldsymbol{\gamma}_\alpha(\boldsymbol{x},\boldsymbol{y})+\boldsymbol{\gamma}_\alpha(\boldsymbol{y},\boldsymbol{x}))/2$ is always symmetric although $\gamma_\alpha(\boldsymbol{x},\boldsymbol{y})$ isn't. Then the first term in the right-hand side of (4.10) satisfies

$$\begin{aligned}J_1 &= \frac{1}{2}\int_\Omega\int_\Omega (u(\boldsymbol{x})-u(\boldsymbol{y}))^2\,\frac{\boldsymbol{\gamma}_\alpha(\boldsymbol{x},\boldsymbol{y})+\boldsymbol{\gamma}_\alpha(\boldsymbol{y},\boldsymbol{x})}{2}\,d\boldsymbol{y}d\boldsymbol{x}\\ &\ge \frac{1}{2}\int_\Omega\int_{\Omega_c} (u(\boldsymbol{x})-u(\boldsymbol{y}))^2\,\frac{\boldsymbol{\gamma}_\alpha(\boldsymbol{x},\boldsymbol{y})+\boldsymbol{\gamma}_\alpha(\boldsymbol{y},\boldsymbol{x})}{2}\,d\boldsymbol{y}d\boldsymbol{x}\\ &= \frac{1}{2}\int_\Omega u^2(\boldsymbol{x})\int_{\Omega_c}\frac{\boldsymbol{\gamma}_\alpha(\boldsymbol{x},\boldsymbol{y})+\boldsymbol{\gamma}_\alpha(\boldsymbol{y},\boldsymbol{x})}{2}\,d\boldsymbol{y}d\boldsymbol{x}\\ &\ge \frac{K_2(\delta)}{4}\|u\|^2_{L^2(\Omega)}.\end{aligned} \tag{4.11}$$

Using the assumption (4.5) and the equality

$$\int_\Omega\int_\Omega u(\boldsymbol{x})u(\boldsymbol{y})\frac{\boldsymbol{\gamma}_\alpha(\boldsymbol{x},\boldsymbol{y})-\boldsymbol{\gamma}_\alpha(\boldsymbol{y},\boldsymbol{x})}{2}d\boldsymbol{y}d\boldsymbol{x} = 0,$$

we obtain for the second term in the right-hand side of (4.10)

$$\begin{aligned}J_2 &= \int_\Omega\int_\Omega u^2(\boldsymbol{x})\frac{\boldsymbol{\gamma}_\alpha(\boldsymbol{x},\boldsymbol{y})-\boldsymbol{\gamma}_\alpha(\boldsymbol{y},\boldsymbol{x})}{2}\,d\boldsymbol{y}d\boldsymbol{x} - \int_\Omega\int_\Omega u(\boldsymbol{x})u(\boldsymbol{y})\frac{\boldsymbol{\gamma}_\alpha(\boldsymbol{x},\boldsymbol{y})-\boldsymbol{\gamma}_\alpha(\boldsymbol{y},\boldsymbol{x})}{2}\,d\boldsymbol{y}d\boldsymbol{x}\\ &= \int_\Omega u^2(\boldsymbol{x})\int_{\Omega_c}\frac{\boldsymbol{\gamma}_\alpha(\boldsymbol{x},\boldsymbol{y})-\boldsymbol{\gamma}_\alpha(\boldsymbol{y},\boldsymbol{x})}{2}\,d\boldsymbol{y}d\boldsymbol{x} \ge 0.\end{aligned} \tag{4.12}$$

The combination of (4.11) and (4.12) gives us

$$\mathbf{B}(u,u) \ge \frac{K_2(\delta)}{4}\|u\|^2_{L^2(\Omega)}.$$

Thus, by the Lax-Milgram theorem, there exists a unique weak solution $u \in L^2_{n0}(\Omega)$ for the nonlocal diffusion problem (3.16). Furthermore, since

$$\frac{K_2(\delta)}{4}\|u\|^2_{L^2(\Omega)} \le \boldsymbol{B}(u,u) = |\mathbf{F}(u)| \le \|f\|_{L^2(\Omega)}\|u\|_{L^2(\Omega)}, \tag{4.13}$$

we have the a priori estimate (4.6). □

Remark 1. *Note that* (4.5) *is a sufficient but not necessary condition for the nonlocal diffusion problem* (3.16) *to be well-posed. In the case of* $a^{i,j}(\boldsymbol{x}) \in C^2(\Omega)$*, notice that the classic diffusion operator in non-divergence form also can be written as*

$$-\mathcal{L}u(\boldsymbol{x}) := -\sum_{i,j=1}^{d} a^{i,j}(\boldsymbol{x})\frac{\partial^2 u}{\partial x_i \partial x_j}(\boldsymbol{x}) = -\nabla\cdot(\mathbf{A}(\boldsymbol{x})\nabla u(\boldsymbol{x})) + \mathbf{b}(\boldsymbol{x})\cdot\nabla u(\boldsymbol{x}), \tag{4.14}$$

where $\mathbf{b}(\boldsymbol{x}) = (b^i(\boldsymbol{x}))$ *with* $b^i(\boldsymbol{x}) = \sum_{j=1}^{d}\frac{\partial a^{i,j}}{\partial x_j}(\boldsymbol{x})$*. Thus the condition* (4.5) *can be regarded as an analogue in the nonlocal sense to the well-known condition for the convection velocity*

$$\nabla\cdot\mathbf{b}(\boldsymbol{x}) \le 0, \quad \boldsymbol{x}\in\Omega. \tag{4.15}$$

Lemma 1. (Maximum principle) *If* $\mathcal{L}_{\delta,\alpha}u > 0$ *in* Ω_s*, then a maximum of* u *is only attained in the interaction domain* Ω_c*.*

Proof. Assume that u attains a maximum at $\boldsymbol{x}_0 \in \Omega_s$, then we have

$$\mathcal{L}_{\delta,\alpha}u(\boldsymbol{x}_0) = \int_\Omega (u(\boldsymbol{y}) - u(\boldsymbol{x}_0))\gamma_\alpha(\boldsymbol{x},\boldsymbol{y})\,d\boldsymbol{y}. \tag{4.16}$$

Since $u(\boldsymbol{y}) - u(\boldsymbol{x}_0) \le 0$, it is easy to verify that

$$\int_\Omega \overbrace{(u(\boldsymbol{y}) - u(\boldsymbol{x}_0))}^{\le 0}\overbrace{\frac{2}{\delta^2\sqrt{(2\pi)^n\,|\delta^2\mathbf{A}(\boldsymbol{x_0})|}}\exp\left(-\frac{1}{2}(\boldsymbol{y}-\boldsymbol{x}_0)^T(\delta^2\mathbf{A}(\boldsymbol{x_0}))^{-1}(\boldsymbol{y}-\boldsymbol{x}_0)\right)}^{\ge 0} \le 0, \tag{4.17}$$

which is a contradiction with the assumption of $\mathcal{L}_{\delta,\alpha}u(\boldsymbol{x}_0) > 0$. □

Let us consider the case of the coefficient matrix $\mathbf{A}(\boldsymbol{x})$ being constant. In this case $\gamma_\alpha(\boldsymbol{x},\boldsymbol{y}) = \gamma_\alpha(\boldsymbol{y},\boldsymbol{x})$, and we can further show that the proposed nonlocal diffusion model (3.16) satisfies global mass conservation. Integrating both sides of (3.16) on Ω_s, we have

$$\begin{aligned}-\int_{\Omega_s}\mathcal{L}_{\delta,\alpha}u(\boldsymbol{x})d\boldsymbol{x} &= \int_{\Omega_s}\int_{\Omega_s\cup\Omega_c}(u(\boldsymbol{x}) - u(\boldsymbol{y}))\gamma_\alpha(\boldsymbol{x},\boldsymbol{y})\;d\boldsymbol{y}d\boldsymbol{x}\\ &= \int_{\Omega_s}\int_{\Omega_s}(u(\boldsymbol{x}) - u(\boldsymbol{y}))\gamma_\alpha(\boldsymbol{x},\boldsymbol{y})\,d\boldsymbol{y}d\boldsymbol{x} + \int_{\Omega_s}\int_{\Omega_c}(u(\boldsymbol{x}) - u(\boldsymbol{y}))\gamma_\alpha(\boldsymbol{x},\boldsymbol{y})\,d\boldsymbol{y}d\boldsymbol{x}.\end{aligned} \tag{4.18}$$

Interchanging the variable $\boldsymbol{x}$ and $\boldsymbol{y}$, we get

$$\int_{\Omega_s}\int_{\Omega_s} u(\boldsymbol{x})\gamma_\alpha(\boldsymbol{x},\boldsymbol{y}) - u(\boldsymbol{y})\gamma_\alpha(\boldsymbol{x},\boldsymbol{y})\;d\boldsymbol{y}d\boldsymbol{x}$$

$$= \frac{1}{2}\Big(\int_{\Omega_s}\int_{\Omega_s} (u(\boldsymbol{x}) - u(\boldsymbol{y}))\gamma_\alpha(\boldsymbol{x},\boldsymbol{y}) + (u(\boldsymbol{y}) - u(\boldsymbol{x}))\gamma_\alpha(\boldsymbol{y},\boldsymbol{x})\, d\boldsymbol{y}d\boldsymbol{x}\Big) = 0,$$

which means the flux from Ω_c into itself is zero. Thus we can get

$$-\int_{\Omega_s} \mathcal{L}_{\delta,\alpha} u(\boldsymbol{x}) d\boldsymbol{x} = \int_{\Omega_s}\int_{\Omega_c} (u(\boldsymbol{x}) - u(\boldsymbol{y}))\gamma_\alpha(\boldsymbol{x},\boldsymbol{y})\; d\boldsymbol{y}d\boldsymbol{x}, \tag{4.19}$$

and the *mass conservation* of the proposed nonlocal model is then obtained as

$$\int_{\Omega_s}\int_{\Omega_c} (u(\boldsymbol{x}) - u(\boldsymbol{y}))\gamma_\alpha(\boldsymbol{x},\boldsymbol{y})\; d\boldsymbol{y}d\boldsymbol{x} = \int_{\Omega_s} f(\boldsymbol{x})\, d\boldsymbol{x}. \tag{4.20}$$

Here, the left-hand side term is the nonlocal flux out of Ω into Ω_s, which is a proxy for the interaction between Ω_c and Ω_s, while the right-hand side term is the source from Ω_c, and putting together, they cancel out each other. Note that such mass conservation doesn't hold anymore if $\mathbf{A}(\boldsymbol{x})$ isn't a constant matrix.

5. Numerical discretization

In this section we propose and analyze an efficient linear collocation scheme for discretizing the nonlocal diffusion problem (3.16). We refer to [8] for a comprehensive review of existing numerical methods for nonlocal models.

5.1. A linear collocation discretization scheme

Without loss of generality, suppose a rectangular grid $\mathcal{T}_h$ of the domain Ω is given. Note that the discretization scheme developed below can also be similarly generalized to triangular/tetrahedral meshes with linear interpolation. Let us denote the nodes of $\mathcal{T}_h$ as $\{\boldsymbol{x}_1, \boldsymbol{x}_2, \cdots, \boldsymbol{x}_{N_s}\} \in \Omega_s$ (interior nodes) and $\{\boldsymbol{x}_{N_s+1}, \boldsymbol{x}_{N_s+2}, \cdots, \boldsymbol{x}_{N_s+N_c}\} \in \Omega_c$ (nonlocal boundary nodes). We assume that the grid matches the boundary of Ω_s. Denote by $\phi_i(\boldsymbol{x})$ the standard continuous piecewise bilinear (if $d = 2$) or trilinear (if $d = 3$) basis function at the point $\boldsymbol{x}_i$ and by S_i the support region for each $\phi_i(\boldsymbol{x})$. At each interior node $\boldsymbol{x}_i$ for $i = 1, 2, \cdots, N_s$, we have for the equation (3.16) that

$$-\mathcal{L}_{\delta,\alpha} u(\boldsymbol{x}_i) = \int_{B_{\delta,\mathbf{A},\alpha}(\boldsymbol{x}_i)} (u(\boldsymbol{x}_i) - u(\boldsymbol{y}))\gamma_\alpha(\boldsymbol{x}_i,\boldsymbol{y})\, d\boldsymbol{y}, \tag{5.1}$$

then we approximate it by

$$-\mathcal{L}^h_{\delta,\alpha} u(\boldsymbol{x}_i) := \int_{B_{\delta,\mathbf{A},\alpha}(\boldsymbol{x}_i)} \mathcal{I}_h\left((u(\boldsymbol{x}_i) - u(\boldsymbol{y}))\gamma_\alpha(\boldsymbol{x}_i,\boldsymbol{y})\right)\, d\boldsymbol{y}, \tag{5.2}$$

where $\mathcal{I}_h(\cdot)$ represents the piecewise bilinear (or trilinear) interpolation operator associated with the grid $\mathcal{T}_h$. Note that (5.2) can be further rewritten as

$$-\mathcal{L}^h_{\delta,\alpha} u(\boldsymbol{x}_i) \;\; = \sum_{\boldsymbol{x}_j \in \Omega\,\&\, j\neq i} (u(\boldsymbol{x}_i) - u(\boldsymbol{x}_j))\gamma_\alpha(\boldsymbol{x}_i,\boldsymbol{x}_j) \int_{B_{\delta,\mathbf{A},\alpha}(\boldsymbol{x}_i)} \phi_j(\boldsymbol{y})\, d\boldsymbol{y}. \tag{5.3}$$

Finally, a linear collocation scheme for solving the nonlocal diffusion problem (3.16) can be given as follows: find $(u_h(\boldsymbol{x}_1), \cdots, u_h(\boldsymbol{x}_{N_s}))$ such that

$$-\mathcal{L}^h_{\delta,\alpha} u_h(\boldsymbol{x}_i) = f(\boldsymbol{x}_i), \qquad i = 1, \cdots, N_s. \tag{5.4}$$

Let us define

$$b_{i,j} = -\gamma_\alpha(\boldsymbol{x}_i, \boldsymbol{x}_j) \int_{B_{\delta,\mathbf{A},\alpha}(\boldsymbol{x}_i)} \phi_j(\boldsymbol{y})\, d\boldsymbol{y}, \quad \text{if } j \neq i, \tag{5.5}$$

and

$$b_{i,j} = -\sum_{\boldsymbol{x}_j \in \Omega \,\&\, j \neq i} b_{i,j}, \quad \text{if } j = i, \tag{5.6}$$

for $1 \leq i \leq N_s$ and $1 \leq j \leq N_s + N_c$. Then the resulting linear system from the collocation discretization scheme (5.4) can be expressed by

$$B_h \vec{u}_h = \vec{f}, \tag{5.7}$$

where $\vec{u}_h = (u_h(\boldsymbol{x}_1), \cdots, u_h(\boldsymbol{x}_{N_s}))^T$, $\vec{f} = (f_1, \cdots, f_{N_s})^T$ with $B_h = (b_{i,j})_{N_s \times N_s}$ and

$$f_i = f(\boldsymbol{x}_i) + \sum_{j=N_s+1}^{N_s+N_c} g(\boldsymbol{x}_j) b_{i,j}. \tag{5.8}$$

It is worth noting that the bandwidth of the stiffness matrix B_h is related to (3.13):

$$B_{\delta,\mathbf{A},\alpha}(\boldsymbol{x}) = \{\boldsymbol{y} \mid (\boldsymbol{y} - \boldsymbol{x})^T \mathbf{A}(\boldsymbol{x})^{-1} (\boldsymbol{y} - \boldsymbol{x}) \leq \delta^2 \chi^2_\alpha(d)\}, \tag{5.9}$$

i.e., the bandwidth of the stiffness matrix B_h is related to the truncation range and the coefficient matrix $\mathbf{A}(\boldsymbol{x})$. The larger $\chi^2_\alpha(d)$, the larger the bandwidth of the stiffness matrix. Similarly, the larger the eigenvalue of $\mathbf{A}(\boldsymbol{x})$, the larger the bandwidth of the stiffness matrix.

Theorem 2. *The stiffness matrix B_h defined in* (5.6) *is a nonsingular M-matrix. Consequently, the linear system* (5.7) *produced from the collocation discretization* (5.4) *for the nonlocal diffusion problem* (3.16) *is uniquely solvable, and u_h always satisfies the following discrete maximum principle when $g = 0$: if $f \leq 0$ in Ω_s, then $\max_{1 \leq i \leq N_s} u_h(\boldsymbol{x}_i) \leq 0$, and if $f \geq 0$ in Ω_s, then $\min_{1 \leq i \leq N_s} u_h(\boldsymbol{x}_i) \geq 0$.*

Proof. It is obvious that for $1 \leq i \leq N_s$ and $1 \leq j \leq N_s + N_c$, we have $\gamma_\alpha(\boldsymbol{x}_i, \boldsymbol{x}_j) > 0$ and $\int_{B_{\delta,\mathbf{A},\alpha}(\boldsymbol{x}_i)} \phi_j(\boldsymbol{y})\, d\boldsymbol{y} > 0$ if $i \neq j$ and $B_{\delta,\mathbf{A},\alpha}(\boldsymbol{x}_i) \cap S_j \neq \emptyset$. Thus by (5.6), it holds that for any $j \neq i$, we have $b_{i,j} < 0$ if $B_{\delta,\mathbf{A},\alpha}(\boldsymbol{x}_i) \cap S_j \neq \emptyset$ and $b_{i,j} = 0$ if $B_{\delta,\mathbf{A},\alpha}(\boldsymbol{x}_i) \cap S_j = \emptyset$ (since $\phi_j(\boldsymbol{y}) = 0$ for $\boldsymbol{y} \notin S_j$). Consequently we have $b_{i,i} > 0$ for $1 \leq i \leq N_s$. Furthermore, it is easy to see that $\sum_{j=1}^{N_s} b_{i,j} > 0$ if $B_{\delta,\mathbf{A},\alpha}(\boldsymbol{x}_i) \cap \Omega_c \neq \emptyset$. Thus, the stiffness matrix B_h is an M-matrix, which means that B_h^{-1} exists and does not have negative entries. The unique solvability of the linear system (5.7) and the discrete maximum principle then directly follows. □

Theorem 2 guarantees the numerical stability of the proposed linear collocation discretization scheme (5.4). In the proposed model, the influence region $B_{\delta,\mathbf{A},\alpha}(\boldsymbol{x}_i)$ of each node $\boldsymbol{x}_i$, is a rotated ellipse. The intersection between $B_{\delta,\mathbf{A},\alpha}(\boldsymbol{x}_i)$ and the support region S_j of another node $\boldsymbol{x}_j$ may be irregular, especially when $\boldsymbol{x}_j$ is near the edge of $B_{\delta,\mathbf{A},\alpha}(\boldsymbol{x}_i)$. This irregular intersection could introduce quadrature errors and potentially impact the accuracy of the simulation. To address this issue, we expand the integral region from the irregular intersection $B_{\delta,\mathbf{A},\alpha}(\boldsymbol{x}_i) \cap S_j$ to the regular support domain S_j. This expansion allows for easy integration by aligning the integration area precisely with the grid.

5.2. Discussion on convergence and asymptotic compatibility

Let us assume that the parameter α is small enough so that *the difference between the original operator* $\mathcal{L}_\delta$ (3.4) *and the truncated operator* $\mathcal{L}_{\delta,\alpha}$ (3.15) *is negligible*. We first consider a rectangular grid $\mathcal{T}_h$ of Ω which is uniform along each space direction with respective grid sizes. If we extend the grid to the whole space $\mathbb{R}^d$, then

$$-\mathcal{L}_\delta^h u(\boldsymbol{x}_i) := \int_{\mathbb{R}^d} \mathcal{I}_h \left((u(\boldsymbol{x}_i) - u(\boldsymbol{y}))\gamma(\boldsymbol{x}_i, \boldsymbol{y}) \right) d\boldsymbol{y},$$

in fact gives the trapezoidal rule for evaluating the original nonlocal diffusion operator (3.2) (no truncation of the influence region)

$$\begin{aligned} -\mathcal{L}_\delta u(\boldsymbol{x}_i) &= \int_{\mathbb{R}^d} (u(\boldsymbol{x}_i) - u(\boldsymbol{y}))\gamma(\boldsymbol{x}_i, \boldsymbol{y})\, d\boldsymbol{y} \\ &= \frac{2}{\delta^2} \int_{\mathbb{R}^d} (u(\boldsymbol{x}_i) - u(\boldsymbol{y})) \frac{1}{\sqrt{(2\pi)^d \left|\delta^2 \mathbf{A}(\boldsymbol{x_i})\right|}} \exp\left(-\frac{(\boldsymbol{y} - \boldsymbol{x}_i)^T \mathbf{A}(\boldsymbol{x}_i)^{-1} (\boldsymbol{y} - \boldsymbol{x}_i)}{2\delta^2} \right) d\boldsymbol{y} \\ &= \frac{2}{\delta^2 \pi^{d/2}} \int_{\mathbb{R}^d} (u(\boldsymbol{x}_i) - u(\boldsymbol{x}_i + \sqrt{2}\delta \mathbf{A}^{1/2} \boldsymbol{y}) \exp\left(-\boldsymbol{y}^T \boldsymbol{y}\right)\, d\boldsymbol{y}. \end{aligned}$$

Based on the analysis results of [43, 18], a remarkable conclusion is that for any fixed horizon parameter $\delta > 0$, such approximation is exponentially convergent with respect to the grid size if u is *analytic* in $\mathbb{R}^d$. Therefore, we expect the numerical solution produced by the linear collocation scheme (5.4) to converge exponentially to the solution of the nonlocal diffusion model (3.16) at the set of all grid points $\{\boldsymbol{x}_i\}$ since $|\mathcal{L}_\delta u(\boldsymbol{x}_i) - \mathcal{L}_{\delta,\alpha} u(\boldsymbol{x}_i)|$ and $|\mathcal{L}_\delta^h u(\boldsymbol{x}_i) - \mathcal{L}_{\delta,\alpha}^h u(\boldsymbol{x}_i)|$ are negligible. On the other hand, if the rectangular grid is not uniform, then the convergence order will downgrade to the regular second-order for linear schemes since the exponential convergence doesn't exist anymore. These results will be numerically demonstrated by experiments in Section 6.1.

Ensuring asymptotic compatibility (i.e., the approximate solution of the nonlocal model problem (3.16) converges to the exact solution of the corresponding local PDE problem (3.11) when the horizon parameter $\delta \to 0$ and the grid size $h \to 0$ simultaneously in arbitrary fashion) is of fundamental importance in guaranteeing the accuracy and reliability of numerical schemes for nonlocal models. In particular, when the ratio between δ and h keeps fixed (i.e., $\delta/h = \kappa$ being a constant) along the grid refinement, it is called the δ-convergence test. This behavior is a manifestation of the well-known continuum limit in which the underlying physical system becomes increasingly smooth and continuous. Although the theoretical proof still remains open, we will numerically show in Section 6.2 that the collocation discretization scheme (5.4) is δ-convergent under a reasonable condition on the ratio κ, in particular, the numerical solution obtained for the nonlocal diffusion model (3.16) will converge quadratically to the solution of the corresponding local problem (3.11) on uniform rectangular grids.

Remark 2. *For the traditional bond-based nonlocal diffusion model, in order to achieve asymptotic compatibility, a popular quadrature-based finite difference discretization for multidimensional problems was developed in [16, 14]: for* $i = 1, \cdots, N_s$,

$$-\widetilde{\mathcal{L}}_{\delta,\alpha}^h u(\boldsymbol{x}_i) := \int_{B_{\delta,\mathbf{A},\alpha}(\boldsymbol{x}_i)} \mathcal{I}_h \left(\frac{u(\boldsymbol{x}_i) - u(\boldsymbol{y})}{W(\boldsymbol{x}_i, \boldsymbol{y})} \right) W(\boldsymbol{x}_i, \boldsymbol{y}) \gamma_\alpha(\boldsymbol{x}_i, \boldsymbol{y})\, d\boldsymbol{y} = f(\boldsymbol{x}_i), \tag{5.10}$$

where the weight function $W(\boldsymbol{x},\boldsymbol{y})$ is usually given by

$$W(\boldsymbol{x},\boldsymbol{y}) = \frac{\|\boldsymbol{y}-\boldsymbol{x}\|^2}{\|\boldsymbol{y}-\boldsymbol{x}\|_1},$$

with the notation $\|\cdot\|_1$ standing for the L^1 norm. However, the numerical scheme (5.10) *could not be asymptotically compatible for our bond-based nonlocal diffusion model* (3.16) *and the original model* (3.4) *developed in this paper. One of the main reasons is that the proof of asymptotic compatibility of the scheme* (5.10) *heavily depends on the radial symmetry (for isotropic diffusion) of the influence region of the kernel function γ_α, which doesn't hold anymore for the case of anisotropic diffusion for the proposed nonlocal model. Numerical tests presented in Section 6.2 will show that the scheme* (5.10) *even fails to be δ-convergent in the case of anisotropic coefficients.*

6. Numerical experiments

In this section, we will conduct various numerical experiments in two and three-dimensional space to showcase application of the proposed bond-based nonlocal diffusion model (3.16), as an approximation to the original nonlocal diffusion model (3.4), to both isotropic and anisotropic diffusion problems, and numerically demonstrate the numerical accuracy and δ-convergence of the proposed linear collocation scheme (5.4). In addition, we also test the discrete maximum principle and the effect of the choice of the truncation parameter $\chi^2_\alpha(d)$ on the approximation accuracy of $\mathcal{L}_{\delta,\alpha}$ to $\mathcal{L}_\delta$. Note that in Examples 1-5 we always take $\chi^2_\alpha(d) = 36$ by default based on the comparison result observed from Example 6 in Subsection 6.4. The choices of $\mathbf{A}(\boldsymbol{x})$ in all examples satisfy the condition (4.5). The solution errors are measured under the *discrete maximum norm*, which is defined to be the maximum absolute value among all grid points $\{\boldsymbol{x}_i\}$.

6.1. Tests with the fixed horizon parameter

We first keep the δ fixed and test the convergence of the linear collocation scheme (5.7) for solving the nonlocal diffusion model (3.16).

Example 1. *Let us take the 2D domain $\Omega_s = [0,1]\times[0,1]$, the isotropic diffusion coefficient matrix $\mathbf{A}_1 = [1,0;0,1]$, and $\delta = 1/40$ for the nonlocal diffusion problem* (3.16). *The exact solution is chosen to be $u(x_1,x_2) = x_1x_2^5$, $u(x_1,x_2) = e^{x_1x_2}$, and $u(x_1,x_2) = \sin(x_1^2+x_2^2)$, respectively. Then the boundary value $g(x_1,x_2)$ is directly obtained from the exact solution $u(x_1,x_2)$ and the source term $f(x_1,x_2)$ are determined accordingly based on the original nonlocal diffusion model* (3.4).

For the coefficient matrix $\mathbf{A}_1$, we have the influence region of the kernel function $\gamma_\alpha(\boldsymbol{x},\boldsymbol{y})$ associated with a point $\boldsymbol{x}\in\Omega_s$ as:

$$B_{\delta,\mathbf{A}_1,\alpha}(\boldsymbol{x}) = \left\{(y_1,y_2)\,\middle|\,\frac{(y_1-x_1)^2}{36}+\frac{(y_2-x_2)^2}{36}\le\delta^2\right\},$$

which corresponds to the disk of radius 6δ centered at $\boldsymbol{x}$. Figure 4-(a) illustrates the computational domain $\Omega = \Omega_s\cup\Omega_c$ and the influence regions for $\mathbf{A}_1$.

In the following, we perform numerical experiments with three types of rectangular grids. Firstly, we uniformly partition the domain to $N\times N$ rectangular cells , where $N = 20, 25, 30, 35, 40, 50$, respectively. The grid spacing are clearly the same for both x- and y- directions, $h_x = h_y = h =$

$1/N$. Table 1 reports the discrete L^∞ solution errors produced by the linear collocation scheme (5.4). We clearly observe the exponential convergence in all three exact solution cases as discussed in Section 5. Furthermore, it is also seen that after $N = 40$ is reached, the errors don't change much anymore or even slightly increase. This is caused by the truncation of the influence region with the parameter $\chi^2_\alpha(2) = 36$ to the original nonlocal model (3.4). The model errors gradually dominate the solution errors along with the mesh refinement.

	$u(x_1,x_2) = x_1x_2^5$		$u(x_1,x_2) = e^{x_1x_2}$		$u(x_1,x_2) = \sin(x_1^2+x_2^2)$	
N	L^∞ error	CR	L^∞ error	CR	L^∞ error	CR
20	3.1594×10^{-2}	-	1.0367×10^{-2}	-	2.0841×10^{-2}	-
25	2.4209×10^{-3}	11.51	8.6355×10^{-4}	11.14	1.9893×10^{-3}	10.53
30	1.2152×10^{-4}	16.41	4.3467×10^{-5}	16.39	1.0027×10^{-4}	16.39
35	3.0658×10^{-6}	23.87	9.5991×10^{-7}	24.74	2.4812×10^{-6}	24.00
40	7.5238×10^{-8}	27.76	9.6315×10^{-8}	17.22	2.8200×10^{-7}	16.29
50	9.5161×10^{-8}	-1.05	5.8425×10^{-8}	2.24	3.1212×10^{-7}	-0.46

Table 1: Numerical results on the discrete L^∞ solution errors and corresponding convergence rates produced by the linear collocation scheme (5.4) for the nonlocal diffusion model (3.16) with fixed $\delta = 1/40$ in Example 1. Uniform rectangular grids of $N \times N$ are used.

Secondly, we divide the domain in the x-direction non-uniformly: $[0, 0.5]$ is partitioned to N_{xl} subintervals and $[0.5, 1)$ N_{xr} subintervals. The y-direction of the domain is then partitioned uniformly into N_y subintervals. Consequently, the obtained rectangular grids are globally non-uniform with $(N_{xl} + N_{xr}) \times N_y$ rectangular cells. Table 2 presents the discrete L^∞ solution errors obtained by using the linear collocation scheme (5.4). We now observe only second-order convergence in all cases as discussed in Section 5.

			$u(x_1,x_2) = x_1x_2^5$		$u(x_1,x_2) = e^{x_1x_2}$		$u(x_1,x_2) = \sin(x_1^2+x_2^2)$	
N_{xl}	N_{xr}	N_y	L^∞ error	CR	L^∞ error	CR	L^∞ error	CR
10	15	20	3.0391×10^{-2}	-	2.2799×10^{-2}	-	1.4295×10^{-2}	-
20	30	40	8.2144×10^{-4}	5.21	1.5704×10^{-3}	3.86	1.1348×10^{-3}	3.66
40	60	80	1.8793×10^{-4}	2.13	3.7312×10^{-4}	2.07	2.7345×10^{-4}	2.05
80	120	160	4.5641×10^{-5}	2.04	9.1977×10^{-5}	2.02	6.7871×10^{-5}	2.01
160	240	320	1.1393×10^{-5}	2.00	2.2804×10^{-5}	2.01	1.6774×10^{-5}	2.01

Table 2: Numerical results on the discrete L^∞ solution errors and corresponding convergence rates with fixed $\delta = 1/40$ produced by the linear collocation scheme (5.4) for the nonlocal diffusion model (3.16) in Example 1. Non-uniform rectangular grids of $(N_{xl} + N_{xr}) \times N_y$ are used.

Example 2. *We still take the 2D domain $\Omega_s = [0, 1] \times [0, 1]$ and $\delta = 1/40$ for the nonlocal diffusion problem* (3.16)*. The exact solution is chosen to be $u(x_1, x_2) = \sin(x_1^2 + x_2^2)$. Then the boundary value $g(x_1, x_2)$ are directly obtained from the exact solution $u(x_1, x_2)$ and the source term $f(x_1, x_2)$ are determined accordingly based on the original nonlocal diffusion model* (3.4)*. Two 2×2 constant anisotropic diffusion coefficient matrices are tested:*

$$\mathbf{A}_2 = \begin{pmatrix} 10 & 0 \\ 0 & 1 \end{pmatrix}, \quad \mathbf{A}_3 = \begin{pmatrix} \cos\frac{\pi}{6} & \sin\frac{\pi}{6} \\ -\sin\frac{\pi}{6} & \cos\frac{\pi}{6} \end{pmatrix} \begin{pmatrix} 10 & 0 \\ 0 & 1 \end{pmatrix} \begin{pmatrix} \cos\frac{\pi}{6} & -\sin\frac{\pi}{6} \\ \sin\frac{\pi}{6} & \cos\frac{\pi}{6} \end{pmatrix}.$$

It is easy to see that the influence region for the coefficient matrix $\mathbf{A}_2$ is given by

$$B_{\delta,\mathbf{A}_2,\alpha}(\boldsymbol{x}) = \left\{ (y_1, y_2) \,\Big|\, \frac{(y_1 - x_1)^2}{360} + \frac{(y_2 - x_2)^2}{36} \le \delta^2 \right\},$$

which is the elliptic region centered at $\boldsymbol{x}$ with the major axis of length $12\sqrt{10}\delta$ and the minor axis of length 12δ. Figure 4-(b) illustrates the computational domain Ω and the influence regions for $\mathbf{A}_2$. The influence area for the coefficient matrix $\mathbf{A}_3$ is given by

$$B_{\delta,\mathbf{A}_3,\alpha}(\boldsymbol{x}) = \left\{ (y_1, y_2) \,\Big|\, \frac{13(y_1 - x_1)^2}{1440} + \frac{\sqrt{3}(y_1 - x_1)(y_2 - x_2)}{80} + \frac{31(y_2 - x_2)^2}{1440} \le \delta^2 \right\}. \tag{6.1}$$

The diagonalization of $\mathbf{A}_3$ shows that $B_{\delta,\mathbf{A}_3,\alpha}(\boldsymbol{x})$ is obtained by rotating the elliptic region corresponding to $\mathbf{A}_2$ with an angle of 30° counterclockwisely. Figure 4-(c) shows the computational domain Ω and the influence regions for $\mathbf{A}_3$. We uniformly partition the domain to $N \times N$ rectangular celles, where $N = 20, 25, 30, 35, 40$ respectively. Table 3 reports the discrete L^∞ solution errors produced by the linear collocation scheme (5.4). We again observe the exponential convergence behavior as that in Example 1 although some oscillations appear in the case of $\mathbf{A}_3$.

	$\mathbf{A}_2$		$\mathbf{A}_3$	
N	L^∞ error	CR	L^∞ error	CR
15	9.7644×10^{-3}	-	1.2143×10^{-3}	-
20	2.0781×10^{-3}	5.38	2.0976×10^{-6}	22.11
25	1.4874×10^{-4}	11.82	2.0492×10^{-7}	10.40
30	9.4193×10^{-6}	15.14	2.0038×10^{-7}	0.12
35	2.4064×10^{-7}	23.79	2.6240×10^{-8}	13.33
40	2.9376×10^{-8}	15.75	1.1368×10^{-7}	-10.98

Table 3: Numerical results on the discrete L^∞ solution errors and corresponding convergence rates produced by the linear collocation scheme (5.4) for the nonlocal diffusion model (3.16) with fixed $\delta = 1/40$ in Example 2. Uniform rectangular grids of $N \times N$ are used.

6.2. Tests for δ-convergence

We now investigate the asymptotic compatibility of the proposed collocation scheme (5.4) as δ and h approach zero simultaneously. Specifically, we consider the so-called δ-convergence test on uniform grids. We compute the error between the numerical solution obtained for the nonlocal problem (3.16) and the exact solution of the corresponding classical local problem (3.11) and observe its behaviors as h tend to zero. By characterizing the δ-convergence of the proposed collocation scheme, we can assess its accuracy and reliability, and gain insight into the underlying physics of the system under consideration. We numerically observe that our scheme is quadratically convergent on uniform rectangular grids when the ratio of the horizon parameter over the grid size satisfies the condition

$$\frac{\delta}{h} \ge \frac{1}{\sqrt{\lambda}}, \tag{6.2}$$

where $\lambda|\boldsymbol{\xi}|^2 \le \boldsymbol{\xi}^T \mathbf{A}(\boldsymbol{x})\boldsymbol{\xi}$ for any $\boldsymbol{\xi} \in \mathbb{R}^d, \boldsymbol{x} \in \Omega$.

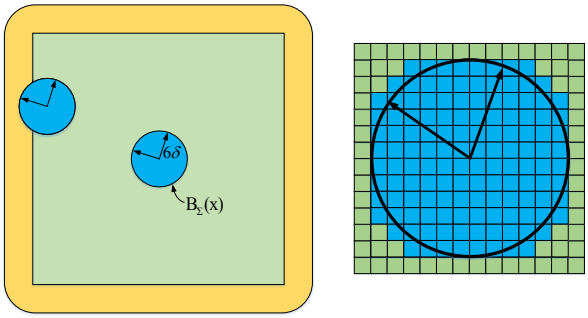

(a) The coefficient matrix $\mathbf{A}_1$

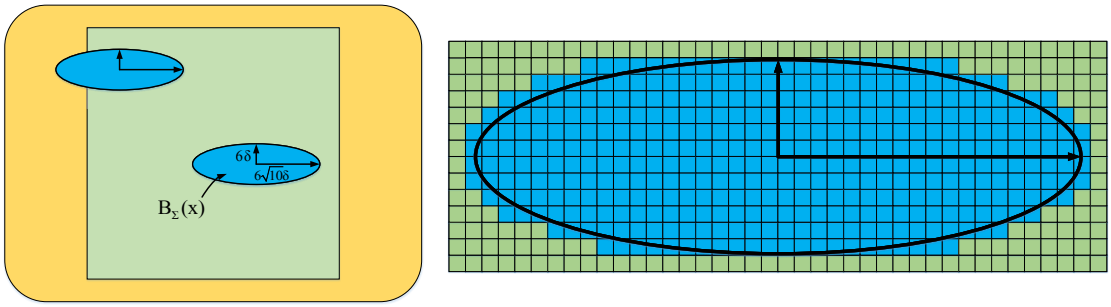

(b) The coefficient matrix $\mathbf{A}_2$

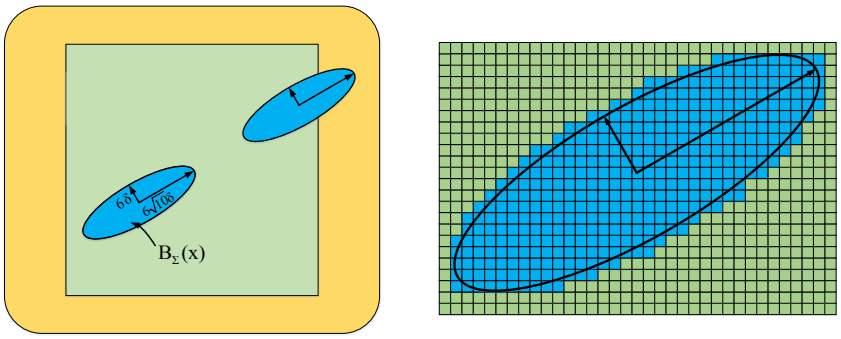

(c) The coefficient matrix $\mathbf{A}_3$

Figure 4: Illustration of the computational domain $\Omega = \Omega_s \cup \Omega_c$ and the influence regions with grids in the background.

Example 3. *We consider the 2D domain* $\Omega_s = [0,1] \times [0,1]$ *and take* $u(x_1, x_2) = \sin(x_1^2 + x_2^2)$ *as the exact solution of the classic diffusion (PDE) problem* (3.11)*. The three different* 2×2 *constant coefficient matrices* $\mathbf{A}_1$*,* $\mathbf{A}_2$ *and* $\mathbf{A}_3$ *defined in Examples 1 and 2 are tested. For the nonlocal diffusion model* (3.16)*, the boundary value* $g(x_1, x_2)$ *is directly obtained from the exact solution* $u(x_1, x_2)$ *and the source term* $f(x_1, x_2)$ *is determined accordingly based on the classic diffusion problem* (3.11)*.*

Table 4 reports the discrete L^∞ solution errors and corresponding convergence rates produced by the linear collocation scheme (5.7) with $\delta = 2h$, $\delta = h$, and $\delta = 0.5h$ respectively. When $\delta = 2h$ and $\delta = h$ which satisfy the ratio condition (6.2), we observe the second-order convergence of the δ-convergence test along the grid refinement. When $\delta = 0.5h$ which violates the ratio condition (6.2),

we still observe the quadratic convergence for the case of $\mathbf{A}_3$, but the results fail to be convergent for the cases of $\mathbf{A}_1$ and $\mathbf{A}_2$.

N	$\mathbf{A}_1$	CR	$\mathbf{A}_2$	CR	$\mathbf{A}_3$	CR
$\delta = 2h$						
40	1.9448×10^{-3}	-	1.6667×10^{-2}	-	1.3550×10^{-2}	-
80	4.7061×10^{-4}	2.04	3.6585×10^{-3}	2.18	2.9302×10^{-3}	2.20
160	1.1569×10^{-4}	2.02	8.5145×10^{-4}	2.10	6.8036×10^{-4}	2.11
320	2.8669×10^{-5}	2.01	2.0433×10^{-4}	2.06	1.7019×10^{-4}	2.00
$\delta = h$						
40	4.8765×10^{-4}	-	3.5896×10^{-3}	-	2.8574×10^{-3}	-
80	1.1504×10^{-4}	2.08	8.4238×10^{-4}	2.09	6.7127×10^{-4}	2.09
160	2.8346×10^{-5}	2.02	2.0492×10^{-4}	2.04	1.5967×10^{-4}	2.07
320	6.6997×10^{-6}	2.08	4.5901×10^{-5}	2.16	3.9727×10^{-5}	2.01
$\delta = 0.5h$						
40	2.1182×10^{-2}	-	1.4436×10^{-3}	-	6.8538×10^{-4}	-
80	2.1088×10^{-2}	0.01	1.4772×10^{-3}	-0.03	1.6219×10^{-4}	2.08
160	2.1026×10^{-2}	0.00	1.5628×10^{-3}	-0.08	4.1364×10^{-5}	1.97
320	2.1070×10^{-2}	0.00	1.6113×10^{-3}	-0.04	1.1121×10^{-5}	1.89

Table 4: Numerical results on the discrete L^∞ solution errors and corresponding convergence rates produced by the linear collocation scheme (5.4) for the nonlocal diffusion model (3.16) with $\delta = 2h$, $\delta = h$, and $\delta = 0.5h$ in Example 3. Uniform rectangular grids of $N \times N$ are used.

For comparison purpose, the numerical results for the case of $\delta = h$ obtained using the quadrature-based finite difference discretization (5.10) on uniform grids are also presented in Table 5. It is evident from the results that the scheme (5.10) produces second-order convergence for the isotropic diffusion case ($\mathbf{A}_1$), but fails to converge for the anisotropic diffusion cases ($\mathbf{A}_2$ and $\mathbf{A}_3$) as discussed in Remark 2.

N	$\mathbf{A}_1$	CR	$\mathbf{A}_2$	CR	$\mathbf{A}_3$	CR
40	5.7139×10^{-4}	-	4.1611×10^{-3}	-	4.4236×10^{-3}	-
80	1.3425×10^{-4}	2.09	1.8107×10^{-3}	1.20	2.3123×10^{-3}	0.94
160	3.3151×10^{-5}	2.02	1.3431×10^{-3}	0.43	1.8423×10^{-3}	0.33
320	7.8984×10^{-6}	2.07	1.2238×10^{-3}	0.13	1.7201×10^{-3}	0.10

Table 5: Numerical results on the discrete L^∞ solution errors and corresponding convergence rates produced by the quadrature-based finite difference discretization scheme (5.10) for the nonlocal diffusion model (3.16) with $\delta = h$ in Example 3. Uniform rectangular grids of $N \times N$ are used.

Example 4. *We consider the 3D domain* $\Omega_s = [0,1] \times [0,1] \times [0,1]$ *and take* $u(x_1, x_2, x_3) = \sin(x_1^2 + x_2^2 + x_3^2)$ *as the exact solution of the classic diffusion (PDE) problem* (3.11)*. The following*

three different 3×3 *constant coefficient matrices are tested:*

$$\mathbf{A}_1 = \begin{pmatrix} 1 & 0 & 0 \\ 0 & 1 & 0 \\ 0 & 0 & 1 \end{pmatrix}, \qquad \mathbf{A}_2 = \begin{pmatrix} 4 & 0 & 0 \\ 0 & 1 & 0 \\ 0 & 0 & 1 \end{pmatrix},$$

and

$$\mathbf{A}_3 = \begin{pmatrix} \cos\frac{\pi}{4} & -\sin\frac{\pi}{4} & 0 \\ \sin\frac{\pi}{4} & \cos\frac{\pi}{4} & 0 \\ 0 & 0 & 1 \end{pmatrix} \cdot \begin{pmatrix} 4 & 0 & 0 \\ 0 & 1 & 0 \\ 0 & 0 & 1 \end{pmatrix} \begin{pmatrix} \cos\frac{\pi}{4} & \sin\frac{\pi}{4} & 0 \\ -\sin\frac{\pi}{4} & \cos\frac{\pi}{4} & 0 \\ 0 & 0 & 1 \end{pmatrix}.$$

For the nonlocal diffusion model (3.16)*, the boundary value* $g(x_1, x_2, x_3)$ *are directly obtained from the exact solution* $u(x_1, x_2, x_3)$ *and the source term* $f(x_1, x_2, x_3)$ *are determined accordingly based on the classic diffusion problem* (3.11)*.*

In this example, the influence region for the isotropic diffusion coefficient matrix $\mathbf{A}_1$ associated with a point $\boldsymbol{x} \in \Omega_s$ is given by

$$B_{\delta,\mathbf{A}_1,\alpha}(\boldsymbol{x}) = \left\{ (y_1, y_2, y_3) \,\middle|\, \frac{(y_1 - x_1)^2}{36} + \frac{(y_2 - x_2)^2}{36} + \frac{(y_3 - x_3)^2}{36} \le \delta^2 \right\},$$

which corresponds to the ball of radius 6δ centered at $\boldsymbol{x}$. The influence region for the anisotropic diffusion coefficient matrix $\mathbf{A}_2$ is given by

$$B_{\delta,\mathbf{A}_2,\alpha}(\boldsymbol{x}) = \left\{ (y_1, y_2, y_3) \,\middle|\, \frac{(y_1 - x_1)^2}{144} + \frac{(y_2 - x_2)^2}{36} + \frac{(y_3 - x_3)^2}{36} \le \delta^2 \right\},$$

which is the ellipsoid region centered at $\boldsymbol{x}$ with the three axises of length 24δ, 12δ, and 12δ, respectively. The influence area for the coefficient matrix $\mathbf{A}_3$ is given by

$$B_{\delta,\mathbf{A}_3,\alpha}(\boldsymbol{x}) = \left\{ (y_1, y_2, y_3) \,\middle|\, \frac{5(y_1 - x_1)^2}{288\delta^2} - \frac{(y_1 - x_1)(y_2 - x_2)}{48} + \frac{5(y_2 - x_2)^2}{288} + \frac{(y_3 - x_3)^2}{36} \le \delta^2 \right\}. \tag{6.3}$$

The diagonalization of $\mathbf{A}_3$ shows that $B_{\delta,\mathbf{A}_3,\alpha}(\boldsymbol{x})$ can be obtained by rotating the ellipsoid region corresponding to $\mathbf{A}_2$ clockwisely with an angle of 45° along the z-axis. We divide the domain Ω_s into a uniform grid of $N \times N \times N$ cells with the grid size $h = 1/N$, where $N = 20, 30, 40, 50$, respectively. We set $\delta = h$ on all level of grids, which satisfies the ratio assumption (6.2). Table 6 reports the discrete L^∞ solution errors and corresponding convergence rates produced by the linear collocation scheme (5.7). We again observe the second-order convergence along the refinement for these δ-convergence tests.

Example 5. *In this example we consider the case of variable diffusion coefficient matrix. We consider the 2D domain* $\Omega_s = [0, 1] \times [0, 1]$ *and take* $u(x_1, x_2) = \sin(x_1^2 + x_2^2)$ *as the exact solution of the classic diffusion (PDE) problem* (3.11)*. The following two different variable* 2×2 *coefficient matrices are considered:*

$$\mathbf{A}_1(x_1, x_2) = \begin{pmatrix} k_1(x_1, x_2) & 0 \\ 0 & k_2(x_1, x_2) \end{pmatrix}$$

N	$\mathbf{A}_1$	CR	$\mathbf{A}_2$	CR	$\mathbf{A}_3$	CR
20	2.4291×10^{-3}	-	6.1233×10^{-3}	-	6.9361×10^{-3}	-
30	1.0677×10^{-3}	2.03	2.7587×10^{-3}	1.97	3.041×10^{-3}	2.03
40	6.1470×10^{-4}	1.92	1.4588×10^{-3}	2.21	1.6902×10^{-3}	2.04
50	3.8099×10^{-4}	2.14	9.2431×10^{-4}	2.05	1.0767×10^{-3}	2.02

Table 6: Numerical results on the discrete L^∞ solution errors and corresponding convergence rates produced by the linear collocation scheme (5.4) for the nonlocal diffusion model (3.16) with $\delta = h$ in Example 4. Uniform rectangular grids of $N \times N \times N$ are used.

and

$$\mathbf{A}_2(x_1, x_2) = \begin{pmatrix} \cos\frac{5\pi}{12} & \sin\frac{5\pi}{12} \\ -\sin\frac{5\pi}{12} & \cos\frac{5\pi}{12} \end{pmatrix} \begin{pmatrix} k_1(x_1, x_2) & 0 \\ 0 & k_2(x_1, x_2) \end{pmatrix} \begin{pmatrix} \cos\frac{5\pi}{12} & -\sin\frac{5\pi}{12} \\ \sin\frac{5\pi}{12} & \cos\frac{5\pi}{12} \end{pmatrix},$$

where $k_1(x_1, x_2) = 4 - 2x_1^2 - x_2^2$ *and* $k_2(x, x_2) = 4 - x_1^2 - 2x_2^2$. *For the nonlocal diffusion model* (3.16)*, the boundary value* $g(x_1, x_2)$ *is directly obtained from the exact solution* $u(x_1, x_2)$ *and the source term* $f(x_1, x_2)$ *are determined accordingly based on the classic diffusion problem* (3.11).

The shape of the influence region associated with a point in Ω_s varies from place to place in this example. For example, for $\mathbf{A}_1(x_1, x_2)$, the influence regions at the point $(1, 1)$ and $(0, 0)$ are a circle, but the influence at the point $(0, 1)$ is an elliptic region. The influence region of $\mathbf{A}_2(x_1, x_2)$ can be obtained by counterclockwisely rotating the influence region corresponding to $\mathbf{A}_1(x, y)$ with an angle of 75°. We use a uniform grid of $N \times N$ cells with the grid size $h = 1/N$, where $N = 40, 80, 160, 320$, respectively. We again set $\delta = h$ on all level of grids, which satisfies the ratio assumption (6.2). Table 7 reports the discrete L^∞ solution errors and corresponding convergence rates produced by the linear collocation scheme (5.4). We again observe the second-order convergence along the refinement for these δ-convergence test cases although the diffusion coefficient matrices are varying now.

N	$\mathbf{A}_1(x_1, x_2)$	CR	$\mathbf{A}_2(x_1, x_2)$	CR
40	1.4229×10^{-3}	-	1.4595×10^{-3}	-
80	3.5517×10^{-4}	2.00	3.6506×10^{-4}	2.00
160	8.5297×10^{-5}	2.06	8.9876×10^{-5}	2.02
320	2.0096×10^{-5}	2.09	2.5342×10^{-5}	1.83

Table 7: Numerical results on the discrete L^∞ solution errors and corresponding convergence rates produced by the linear collocation scheme (5.4) for the nonlocal diffusion model (3.16) with $\delta = h$ in Example 5. Note that the two diffusion coefficient matrices are varying. Uniform rectangular grids of $N \times N \times N$ are used

6.3. Tests for discrete maximum principle

In this subsection we test the discrete maximum principle of the linear collocation scheme (5.7).

Example 6. *We take the 2D domain* $\Omega_s = [0, 1] \times [0, 1]$ *and* $\delta = 1/40$ *for the nonlocal diffusion problem* (3.16)*. Four different* 2×2 *coefficient matrices (two constant and two variable matrices)*

are considered:

$$\mathbf{A}_1 = \begin{pmatrix} 10 & 0 \\ 0 & 1 \end{pmatrix},$$

$$\mathbf{A}_2 = \begin{pmatrix} \cos\frac{\pi}{6} & \sin\frac{\pi}{6} \\ -\sin\frac{\pi}{6} & \cos\frac{\pi}{6} \end{pmatrix} \begin{pmatrix} 10 & 0 \\ 0 & 1 \end{pmatrix} \begin{pmatrix} \cos\frac{\pi}{6} & -\sin\frac{\pi}{6} \\ \sin\frac{\pi}{6} & \cos\frac{\pi}{6} \end{pmatrix},$$

$$\mathbf{A}_3(x_1, x_2) = \begin{pmatrix} k_1(x_1, x_2) & 0 \\ 0 & k_2(x_1, x_2) \end{pmatrix},$$

$$\mathbf{A}_4(x_1, x_2) = \begin{pmatrix} \cos\frac{5\pi}{12} & \sin\frac{5\pi}{12} \\ -\sin\frac{5\pi}{12} & \cos\frac{5\pi}{12} \end{pmatrix} \begin{pmatrix} k_1(x_1, x_2) & 0 \\ 0 & k_2(x_1, x_2) \end{pmatrix} \begin{pmatrix} \cos\frac{5\pi}{12} & -\sin\frac{5\pi}{12} \\ \sin\frac{5\pi}{12} & \cos\frac{5\pi}{12} \end{pmatrix},$$

where $k_1(x_1, x_2) = 4 - 2x_1^2 - x_2^2$ *and* $k_2(x_1, x_2) = 4 - x_1^2 - 2x_2^2$. *In this example, we impose a Dirichlet boundary condition on* Ω_c *as follows:* $u(x_1, x_2) = 1$ *if* $x_1 \le 0$ *or* $x_2 \le 0$ *and* $u(x_1, x_2) = 0$ *otherwise. The source term is chosen as* $f(x_1, x_2) = 0$. *Although the exact solution of the nonlocal diffusion problem* (3.16) *is unknown, we know its value must fall between 0 and 1.*

We take a uniform grid of 80×80 and solve the nonlocal model using the linear collocation scheme (5.7). Figure 5 plots the numerical solutions produced with these four different coefficient matrices. We can see that the discrete maximum principle is well preserved in all cases.

6.4. Effect of $\chi_\alpha^2(d)$ *on the model approximation of* $\mathcal{L}_{\delta,\alpha}$ *to* $\mathcal{L}_\delta$

In this subsection, we test the effect of the choice of $\chi_\alpha^2(d)$ on the accuracy of the truncated nonlocal diffusion operator $\mathcal{L}_{\delta,\alpha}$ defined in (3.15) as an approximation of the original nonlocal diffusion operator $\mathcal{L}_\delta$ defined in (3.2).

Example 7. *We take exactly the same experimental settings as those of Example 3, except that we now test different values of* $\chi_\alpha^2(2)$. *Specifically, we choose* $\chi_\alpha^2(d) = 9, 16, 25, 26, 49$, *respectively.*

We take a uniform grid of $N \times N$ cells with the grid size $h = 1/N$, where $N = 40, 80, 160$ respectively. Table 8 reports the numerical results on the discrete L^∞ solution errors produced by the linear collocation scheme (5.4) for the nonlocal diffusion model (3.16) with $\delta = h$ under different choices of $\chi_\alpha^2(2)$. We can see from Table 8 that the solution errors decrease and converge rapidly along with the increasing of $\chi_\alpha^2(2)$ from 9 to 49, and the differences of solution errors between $\chi_\alpha^2(2) = 36$ and $\chi_\alpha^2(2) = 49$ are almost negligible. Therefore, we suggest the selection of $\chi_\alpha^2(2) = 36$ in practice, in order to ensure the model accuracy of the truncated nonlocal diffusion model (3.16) while still maintaining the efficiency of numerical simulations.

7. Conclusions

This paper presents a novel bond-based nonlocal diffusion model with matrix-valued coefficients in non-divergence form. Our approach involves integrating the coefficient matrix into the covariance matrix and employing the multivariate Gaussian function with truncation as the kernel function to accurately encapsulate the diffusion process. Substantiating the robustness of our model, we establish its well-posedness along with elucidating certain inherent properties. To numerically

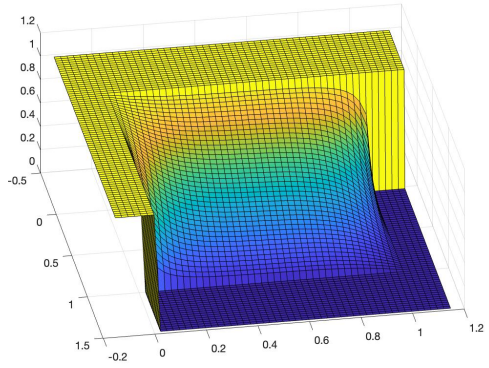

(a) The coefficient matrix $\mathbf{A}_1$

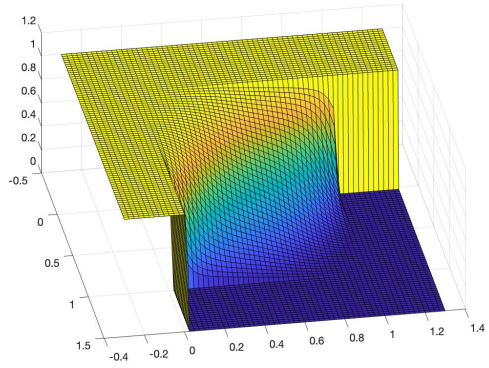

(b) The coefficient matrix $\mathbf{A}_2$

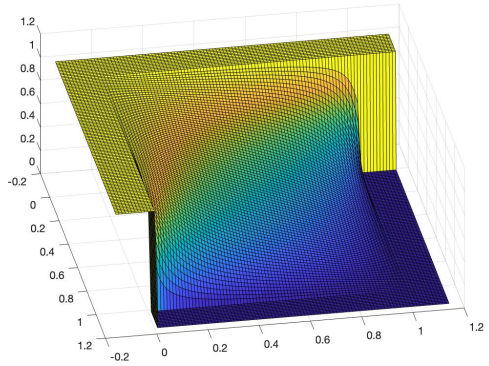

(c) The coefficient matrix $\mathbf{A}_3(x_1, x_2)$

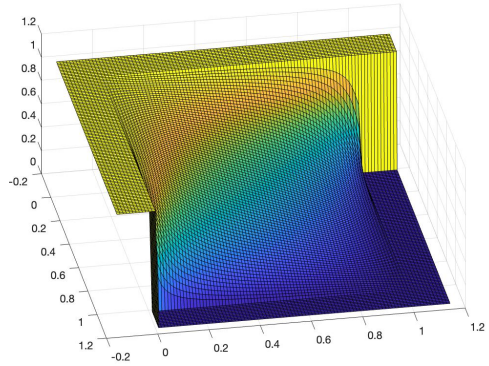

(d) The coefficient matrix $\mathbf{A}_4(x_1, x_2)$

Figure 5: Numerical solutions produced by the linear collocation scheme (5.4) for the nonlocal diffusion model (3.16) with the four different diffusion coefficient matrices in Example 6. Uniform rectangular grids of $N \times N$ are used.

solve the model, we also design an efficient linear collocation discretization scheme. Extensive experiments are conducted in two and three dimensions to showcase the versatility of our model in addressing various isotropic and anisotropic diffusion problems. The numerical results demonstrate high-order accuracy of the proposed collocation scheme for solving the proposed nonlocal diffusion model, and furthermore, we also numerically observe the δ-convergence of our scheme on uniform rectangular grids under a reasonable condition on the ratio δ/h.

On the other hand, there are also many interesting problems on needed to further investigated. Firstly, it remains an open question on how to rigorously prove the observed conditional δ-convergence of the proposed collocation scheme and what the exact condition is to guarantee the complete δ-convergence. Secondly, an intriguing question is whether and how one can appropriately modify the classic quadrature-based finite difference scheme to recover its δ-convergence and even asymptotic compatibility. Finally, it is also highly desired to generalize the proposed work to develop bond-based nonlocal diffusion and convection-diffusion models in conservative or divergence form.

	$\mathbf{A}_1 = [1, 0, 0; 1]$				
N	$\chi^2_\alpha(2) = 9$	$\chi^2_\alpha(2) = 16$	$\chi^2_\alpha(2) = 25$	$\chi^2_\alpha(2) = 36$	$\chi^2_\alpha(2) = 49$
40	6.3785×10^{-2}	9.7359×10^{-4}	4.7136×10^{-4}	4.8765×10^{-4}	4.6316×10^{-4}
80	1.0611×10^{-2}	6.8071×10^{-4}	1.2696×10^{-4}	1.1503×10^{-4}	1.1788×10^{-4}
160	1.0517×10^{-2}	8.9142×10^{-4}	4.2278×10^{-5}	2.8346×10^{-5}	2.8360×10^{-5}
	$\mathbf{A}_2 = [10, 0, 0; 1]$				
N	$\chi^2_\alpha(2) = 9$	$\chi^2_\alpha(2) = 16$	$\chi^2_\alpha(2) = 25$	$\chi^2_\alpha(2) = 36$	$\chi^2_\alpha(2) = 49$
40	1.7101×10^{-2}	4.0173×10^{-3}	3.7986×10^{-3}	3.5896×10^{-3}	3.5861×10^{-3}
80	1.3309×10^{-2}	1.3378×10^{-3}	8.4862×10^{-4}	8.4238×10^{-4}	8.4376×10^{-4}
160	1.2548×10^{-2}	7.5558×10^{-4}	2.0819×10^{-5}	2.0492×10^{-5}	2.0315×10^{-5}
	$\mathbf{A}_3 = [31/4, -9\sqrt{3}/4; -9\sqrt{3}/4, 13/4]$				
N	$\chi^2_\alpha(2) = 9$	$\chi^2_\alpha(2) = 16$	$\chi^2_\alpha(2) = 25$	$\chi^2_\alpha(2) = 36$	$\chi^2_\alpha(2) = 49$
40	1.6155×10^{-2}	3.3413×10^{-3}	2.8710×10^{-3}	2.8574×10^{-3}	2.8573×10^{-2}
80	1.3834×10^{-2}	1.1772×10^{-3}	6.8493×10^{-4}	6.7127×10^{-4}	6.7122×10^{-4}
160	1.3154×10^{-2}	6.8957×10^{-4}	1.7647×10^{-4}	1.6276×10^{-4}	1.6276×10^{-4}

Table 8: Numerical results on the discrete L^∞ solution errors with fixed $\delta = h$ produced by the linear collocation scheme (5.4) for the nonlocal diffusion model (3.16) under different choices of $\chi^2_\alpha(d)$ in Example 7. Uniform rectangular grids of $N \times N$ are used.

References

[1] F. Bobaru and M. Duangpanya, The peridynamic formulation for transient heat conduction, *Int. J. Heat Mass Transf.*, **53**, pp. 4047-4059, 2010.

[2] F. Bobaru and M. Duangpanya, A peridynamic formulation for transient heat conduction in bodies with evolving discontinuities, *J. Comput. Phys.*, **231**, pp. 2764-2785, 2012.

[3] S.C. Brenner, T. Gudi, M. Neilan and L.-Y. Sung, C^0penalty methods for the fully nonlinear Monge-Ampère equation, *Math. Comp.*, **80**, pp. 1979-1995, 2011

[4] J. K. Blitzstein and J. Hwang, Introduction to Probability, *Chapman & Hall(CRC press)*, 2019.

[5] L. Caffarelli and C. E. Gutiérrez, Properties of the solutions of the linearized Monge-Ampère equation, *Am. J. Math.*, **119**, pp. 423-465, 1997.

[6] W. Chen, X. Gu, Q. Zhang and X. Xia, A refined thermo-mechanical fully coupled peridynamics with application to concrete cracking, *Eng. Fract. Mech.*, **242**, 107463, 2021.

[7] H. Chen and D. Liu, Formulation of a nonlocal discrete model for anisotropic heat conduction problems, *Int. J. Therm. Sci.*, **182**, 107816, 2022.

[8] M. D'Elia, Q. Du, C. Glusa, M. Gunzburger, X. Tian and Z. Zhou, Numerical methods for nonlocal and fractional models, *Acta Numerica*, **29**, pp. 1-124, 2020.

[9] M. D'elia and M. Gulian, Analysis of anisotropic nonlocal diffusion models: Well-posedness of fractional problems for anomalous transport, *Numer. Math. Theor. Meth. Appl.*, **15**, pp. 851-875, 2022.

[10] M. Dördüncü, Peridynamics for the solution of the steady state heat conduction problem in plates with insulated cracks, *J. Aeronaut. Space. Technol.*, **12**, pp. 145-155, 2019.

[11] Q. Du, Nonlocal Modeling, Analysis, and Computation, *SIAM*, 2019.

[12] Q. Du, M. Gunzburger, R. B. Lehoucq and K. Zhou, Analysis and approximation of nonlocal diffusion problems with volume constraints, *SIAM Rev.*, **54**, pp. 667-696, 2012.

[13] Q. Du, M. Gunzburger, R. B. Lehoucq and K. Zhou, A nonlocal vector calculuts, nonlocal volume-constrained problems, and nonlocal balance laws, *Math. Models Methods Appl. Sci.*, **23**, pp. 493-540, 2013.

[14] Q. Du, L. Ju, and H. Tian, A conservative nonlocal convection–diffusion model and asymptotically compatible finite difference discretization, *Comput. Methods Appl. Mech. Engrg.*, **320**, pp. 46-67, 2017.

[15] Q. Du, L. Ju, L. Tian and K. Zhou, A posteriori error analysis of finite element method for linear nonlocal diffusion and peridynamic models, *Math. Comp.*, **82**, pp. 1889-1922, 2013.

[16] Qiang Du, Y. Tao, X. Tian, and J. Yang. Asymptotically compatible discretization of multidimensional nonlocal diffusion models and approximation of nonlocal green's functions. *IMA J. Numer. Anal.*, **39**, pp. 607-625, 2019.

[17] Q. Du and K. Zhou, Mathematical analysis for the peridynamic nonlocal continuum theory, *ESAIM: Math. Mod. Numer. Anal.*, **45**, pp. 217-234, 2011.

[18] N. Eggert and J. Lund, The trapezoidal rule for analytic functions of rapid decrease, *J. Comput. Appl. Math.*, **27**, pp. 389-406, 1989.

[19] W. H. Fleming and H. Soner, Controlled Markov processes and viscosity solutions, *Springer Science and Business Media*, 2006.

[20] B. Gatmiri and P. Delage, A formulation of fully coupled thermal–hydraulic–mechanical behaviour of saturated porous media—numerical approach, *Int. J. Numer. Analyt. Methods Geomech.*, **21**, pp. 199-225, 1997.

[21] A. Gagani, Y. Fan, A. H. Muliana and A. T. Echtermeyer, Micromechanical modeling of anisotropic water diffusion in glass fiber epoxy reinforced composites, *J. Compos. Mater.*, **52**, pp. 2321-2335, 2018.

[22] Y. Gao, G. Yuan, S. Wang and X. Hang, A finite volume element scheme with a monotonicity correction for anisotropic diffusion problems on general quadrilateral meshes, *J. Comput. Phys.*, **407**, 109143, 2020.

[23] D. Gilbarg and N. S. Trudinger, Elliptic partial differential equations of second order, *Springer*, Berlin, 1977.

[24] M. Gunzburger and R. B. Lehoucq, A nonlocal vector calculus with application to nonlocal boundary value problems, *Multiscale Model. Simul.*, **8**, pp. 1581-1598, 2010.

[25] S. Jafarzadeh, Z. Chen, S. Li and F. Bobaru, A peridynamic mechano-chemical damage model for stress-assisted corrosion, *Electrochim. Acta*, **323**, 134795, 2019.

[26] R. Jabakhanji and R. H. Mohtar, A peridynamic model of flow in porous media, *Adv. Water Resour.*, **78**, pp. 22-35, 2015.

[27] A. Katiyar, J. T. Foster, H. Ouchi and M. M. Sharma, A peridynamic formulation of pressure driven convective fluid transport in porous media, *J. Comput. Phys.*, **261**, pp. 209-229, 2014.

[28] N. Kerber, M. Weiβenhofer, K. Raab, K. Litzius, J. Zázvorka, U. Nowak and M. Kläi, Anisotropic skyrmion diffusion controlled by magnetic-field-induced symmetry breaking, *Phys. Rev. Appl.*, **15**, 044029, 2021.

[29] J. Lv and Y. Li, Optimal biquadratic finite volume element methods on quadrilateral meshes, *SIAM J. Numer. Anal.*, **50**, pp. 2379-2399, 2012.

[30] K. Lan, J. Liu, Z. Li, et. al. , Progress in octahedral spherical hohlraum study, *Matter. Radiat. Extrem.*, **1**, pp. 8-27, 2016.

[31] N.Q. Le, H. Mitake and H. V. Tran, Dynamical and Geometric Aspects of Hamilton-Jacobi and Linearized Monge-Ampère Equations, Springer, New York 2017.

[32] J. Lu, M. Yang and Y. Nie, Convergence analysis of Jacobi spectral collocation methods for weakly singular nonlocal diffusion equationswith volume constraints, *Appl. Math. Comput.*, **431**, 127345, 2022.

[33] Q. Ma and Z. Chen, Numerical study on gas diffusion in isotropic and anisotropic fractal porous media (gas diffusion in fractal porous media), *Int. J. Heat Mass Transf.*, **79**, pp. 925-929, 2014.

[34] M. Neilan, Quadratic finite element methods for the Monge-Ampère equation, *J. Sci. Comput.*, **54**, pp. 200-226, 2013

[35] P. Perona and J. Malik, Scale-space and edge detection using anisotropic diffusion, *IEEE Trans. Pattern Anal. Machine Intell.*, **12**, pp. 629–639, 1990.

[36] G. Ren, J. Liu, W. Huo and K. Lan, Analysis of hohlraum energetics of the SG series and the nif experiments with energy balance model, *Matter. Radiat. Extrem.*, **2**, pp. 22–27, 2017.

[37] S.A. Silling, Reformulation of elasticity theory for discontinuities and long-range forces, *J. Mech. Phys. Solids.*, **48**, pp. 175-209, 2000.

[38] Z. Sheng and G. Yuan, A new nonlinear finite volume scheme preserving positivity for diffusion equations, *J. Comput. Phys.*, **315**, pp. 182-193, 2016.

[39] Z. Sheng and G. Yuan, Construction of nonlinear weighted method for finite volume schemes preserving maximum principle, *SIAM J. Sci. Comput.*, **40**, pp. A607-A628, 2018 .

[40] S.A. Silling and R. B. Lehoucq, Peridynamic theory of solid mechanics, *Adv. Appl. Mech.*, **44**, pp. 73-168, 2010.

[41] Y. Sun and H. Yu, A unified non-local fluid transport model for heterogeneous saturated porous media, *Comput. Methods Appl. Mech. Engrg.*, **389**, 114294, 2022.

[42] N. S. Trudinger and Xu-jia Wang, The Monge-Ampère equation and its geometric applications. Handbook of geometric analysis, **1**, pp. 467-524, 2008.

[43] L.N. Trefethon and J. Weideman, The exponentially convergent trapezoidal rule, *SIAM Rev.*, **56**, pp. 385-458, 2014.

[44] J. L. Vazquez, The Porous Medium Equation: Mathematical Theory, *Oxford University Press*, 2006.

[45] M. Vogel, Fusion: An introduction to the physics and technology of magnetic confinement fusion, *Contemp. Phys.*, **52**, pp. 595-596, 2011.

[46] S. Whitaker, Flow in porous media I: A theoretical derivation of darcy's law, *Transp. Porous Media.*, **1**, pp. 3-25, 1986.

[47] J. Wang, Z. Sheng and G. Yuan, A vertex-centered finite volume scheme preserving the discrete maximum principle for anisotropic and discontinuous diffusion equations, *J. Comput. Appl. Math.*, **402**, 113785, 2022.

[48] Y.-L. You, W. Xu, A. Tannenbaum and M. Kaveh, Behavioral analysis of anisotropic diffusion in image processing, *IEEE T. Image Process.*, **5**, pp. 1539-1553, 1996.

[49] Y. Yu, G. Yuan Z. Sheng and Y. Li, The finite volume scheme preserving maximum principle for diffusion equations with discontinuous coefficient, *Comput. Math. Appl.*, **79**, pp. 2168-2188, 2020.

[50] J. Zhao, S. Jafarzadeh, M. Rahmani, Z. Chen, Y.-R. Kim and F. Bobaru, A peridynamic model for galvanic corrosion and fracture, *Electrochimica Acta*, **391**, 138968, 2021.